ELSEVIER

Journal of Volcanology and Geothermal Research 71 (1996) 73–107

Journal of volcanology and geothermal research

Mount St. Augustine volcano fumarole wall rock alteration: mineralogy, zoning, composition and numerical models of its formation process

Aberra Getahun [a,*], Mark H. Reed [a], Robert Symonds [b]

[a] *Department of Geological Sciences, University of Oregon, Eugene, OR 97403, USA*
[b] *U.S. Geological Survey, Cascades Volcano Observatory, 5400 MacArthur Blvd., Vancouver, WA 98661, USA*

Received 23 May 1994; accepted 2 October 1995

Abstract

Intensely altered wall rock was collected from high-temperature (640°C) and low-temperature (375°C) vents at Augustine volcano in July 1989. The high-temperature altered rock exhibits distinct mineral zoning differentiated by color bands. In order of decreasing temperature, the color bands and their mineral assemblages are: (a) white to grey (tridymite–anhydrite); (b) pink to red (tridymite–hematite–Fe hydroxide–molysite ($FeCl_3$) with minor amounts of anhydrite and halite); and (c) dark green to green (anhydrite–halite–sylvite–tridymite with minor amounts of molysite, soda and potash alum, and other sodium and potassium sulfates). The alteration products around the low-temperature vents are dominantly cristobalite and amorphous silica with minor potash and soda alum, aphthitalite, alunogen and anhydrite.

Compared to fresh 1986 Augustine lava, the altered rocks exhibit enrichments in silica, base metals, halogens and sulfur and show very strong depletions in Al in all alteration zones and in iron, alkali and alkaline earth elements in some of the alteration zones.

To help understand the origins of the mineral assemblages in altered Augustine rocks, we applied the thermochemical modeling program, GASWORKS, in calculations of: (a) reaction of the 1987 and 1989 gases with wall rock at 640 and 375°C; (b) cooling of the 1987 gas from 870 to 100°C with and without mineral fractionation; (c) cooling of the 1989 gas from 757 to 100°C with and without mineral fractionation; and (d) mixing of the 1987 and 1989 gases with air. The 640°C gas–rock reaction produces an assemblage consisting of silicates (tridymite, albite, diopside, sanidine and andalusite), oxides (magnetite and hercynite) and sulfides (bornite, chalcocite, molybdenite and sphalerite). The 375°C gas–rock reaction produces dominantly silicates (quartz, albite, andalusite, microcline, cordierite, anorthite and tremolite) and subordinate amounts of sulfides (pyrite, chalcocite and wurtzite), oxides (magnetite), sulfates (anhydrite) and halides (halite). The cooling calculations produce: (a) anhydrite, halite, sylvite; (b) Cu, Mo, Fe and Zn sulfides; (c) Mg fluoride at high temperature (> 370°C); (d) chlorides, fluorides and sulfates of Mn, Fe, Zn, Cu and Al at intermediate temperature (170–370°C); and (e) hydrated sulfates, liquid sulfur, crystalline sulfur, hydrated sulfuric acid and water at low temperature

* Corresponding author. Present address: Brown and Caldwell, 3636, N Central, Ave., Suite 300, Phoenix, AZ 85012, USA.

SSDI 0377-0273(95)00071-2

(< 170°C). The volcanic gas–air mixing calculation produces major amounts of Na and K sulfates, minor amounts of hematite and trace amounts (< 1%) of anhydrite at log gas/air (lg/a) ratios > 0.41 (> 628°C). This is followed by precipitation of sulfates of Fe, Cu, Pb, Zn and Al at lg/a ratios between 0.41 and −0.4 (628–178°C). At a lg/r ratio of ≤ −0.4 (178°C), anhydrous sulfates are replaced by their hydrated forms and hygroscopic sulfuric acid forms. At these low g/a ratios, hydrated sulfuric acid becomes the dominant phase in the system.

Comparison of the thermochemical modeling results with the natural samples suggests that the alteration assemblages include: (1) minerals that precipitate from direct cooling of the volcanic gas; (2) phases that form by volcanic gases mixing with air; and (3) phases that form by volcanic gas–air–rock reaction. A complex interplay of the three processes produces the observed mineral zoning. Another implication of the numerical simulation results is that most of the observed incrustation and sublimate minerals apparently formed below 700°C.

1. Introduction

Historically, study of volcanic gases has been impaired by the difficulties and dangers of obtaining high-quality samples and by using unsatisfactory sampling and interpretation tools. However, in recent years, burgeoning interest in volcanic pollution (e.g., Lepel et al., 1978; Johnston, 1980; Symonds et al., 1988), the need for an eruption prediction and monitoring technology (e.g., Harris et al., 1981; Casadevall et al., 1983; Toutain et al., 1992; Sutton et al., 1992) and the quest for understanding metal transport in magmatic systems (e.g., Krauskopf, 1964; Symonds et al., 1987, 1992; Quisefit et al., 1989; Reed, 1992) have contributed a great deal to the understanding of volcanic gases. In addition, the advent of new sampling and computational techniques (e.g., Le Guern and Bernard, 1982; Symonds et al., 1987; Le Guern, 1988; Quisefit et al., 1989; Symonds and Reed, 1993) have provided new tools to study volcanic gases.

This study focuses on the gas-phase alteration of wall rock in Mount St. Augustine fumaroles. We analyzed wall rock samples collected from 375–640°C vents in 1989, three years after the 1986 eruptions. Altered wall rocks bordering the 1989 fumaroles exhibit concentric color bands produced by various mineral assemblages that apparently formed from gas–rock reactions and mineral precipitation from cooling gases. Both processes of sublimation and alteration of the wall rocks respond to sharp gradients in temperature and oxygen fugacity around the fumarole orifices (e.g., Keith, 1991).

Incrustations around the low-temperature (< 250°C) rootless fumaroles on the 1986 pyroclastic flows are documented by Kodosky and Keskinen (1990). In this study, we document the high-temperature-alteration mineral assemblages, determine the gains and losses of major, trace and rare earth elements in all alteration zones, and use thermochemical modeling to interpret the origin of the wall rock alteration.

2. Augustine volcano

Mount St. Augustine is located about 285 km southwest of Anchorage, Alaska, in the lower Cook Inlet basin (Fig. 1). The volcano lies about 105 km above the seismically active Benioff zone dipping 45° to the northwest (Kienle and Swanson, 1985). It

Fig. 1. Map of the state of Alaska, USA, showing Augustine island, located in the eastern part of the Aleutian Arc.

is an andesitic–dacitic island volcano that consists of a central dome complex surrounded by an apron of debris avalanche deposits (Beget and Kienle, 1992). The volcanic deposits overlie a sequence of Mesozoic marine and terrestrial sedimentary rocks and Pleistocene glacial deposits (Detterman, 1973; Buffler, 1975).

This symmetrical, cone-shaped volcano is the most active volcano on the eastern Aleutian arc, having erupted in 1812, 1883, 1935, 1963–1964, 1976 and 1986 (Johnston, 1978; Kienle, 1986; Kienle et al., 1986). Following the April 1986 eruption, the hottest fumaroles were located at the base of the spine on the 1986 lava dome (Symonds et al., 1990). Augustine volcano is well known for its Cl-rich volatiles (Johnston, 1980) and owing to intense HCl emissions, the dome fumaroles were inaccessible in 1986 (Symonds et al., 1990). In 1987, they were discharging 870°C gases that were exceptionally enriched in HCl, SO_2 and metals (Symonds et al., 1990). Other fumarole fields in 1986–1989 were located: (a) on the moat (a remnant of the 1976 lava dome); (b) on an area extending from the edge of the 1964 lava dome to the saddle between the 1963 and 1935 lava domes (the solfatara fumarole field); and (c) on the 1986 pyroclastic flows (Kodosky and Keskinen, 1990; Symonds et al., 1990).

3. Previous studies

Earlier investigators of the Augustine volatiles have studied pre-eruption volatiles in the magmas, fumarolic discharges, and gases and aerosols in plumes. Johnston (1978, 1980) analysed glass inclusions and showed that the Augustine magmas were unusually Cl rich. Lepel et al. (1978) studied the enrichment of volatile elements in 1976 eruption plumes. Viglino et al. (1985) used H and O isotope evidence to show that there is a magmatic component in the >450°C, 1976–1982 fumarolic condensates. Kodosky et al. (1991) studied the 1976–1984 gases and showed that, after the 1976 eruption, the gases became increasingly diluted with meteoric H_2O.

During the 1986 explosive eruptions, Rose et al. (1988) measured the fluxes of HCl, SO_2 and ash. They estimated the low-level eruptive emission rates at 10,000 and 24,000 metric tons/day (t/d) for HCl and SO_2, respectively; peak eruptive rates were estimated at 160,000 and 375,000 t/d for HCl and SO_2. By July 1986, three months after the March–April eruptions, SO_2 emission rates had declined to 380 t/d (Rose et al., 1988). After the summer of 1986, SO_2 emission rates continued to decline and by August 1987, they were only 27 t/d (Symonds et al., 1990). Emission rates of other species also declined after the 1986 eruptions (Symonds et al., 1992).

Geochemical surveys of the fumarole fields began in July 1986 when Symonds collected gases and condensates from the moat fumaroles and condensates from the solfatara and 1986 pyroclastic flow fumaroles (Symonds et al., 1990). Gases and condensates were also collected from the dome fumaroles in the summers of 1987, 1989 and 1992 (Symonds et al., 1990; Symonds, unpubl.). The 1987 dome gases, which are most representative of the deep fluids at Augustine, contain extremely high concentrations of HCl and total S, relative to the magma; they are also enriched by factors of 10^7 to 10^2 in Br, B, Cd, As, Bi, Pb, Sb, Mo, Zn, Cu, K, Li and Na (Symonds et al., 1990). Thermochemical modeling by Symonds et al. (1992) indicates that most trace elements in these dome gases are degassed from shallow magma as simple chloride, oxychloride, sulfide and elemental gas species, although some non-volatile elements (e.g., Al, Ti) may originate from entrained rock particles. After 1987, the dome gases became increasingly diluted with meteoric vapor and by 1992, the dome fumaroles contained 99.8% steam (Symonds, unpubl.).

Kodosky and Keskinen (1990) studied the incrustations from low-temperature (<250°C) rootless fumaroles on the 1986 pyroclastic flows. They grouped the pyroclastic-flow incrustations into three color zones: an innermost reddish-orange zone; a greenish-yellow or reddish-green middle zone; and a white outermost zone. They described six crystalline phases including gypsum, anhydrite, native sulfur, tridymite, halite and soda-alum [$NaAl(SO_4)_2 \cdot 12H_2O$] in decreasing order of abundance. Symonds (unpubl.) studied the incrustations surrounding the moat fumaroles. He found similar results to those of Kodosky and Keskinen (1990), except that >400°C vents also had an innermost blue or black zone

containing abundant Zn and Cu sulfates; the black zone also contained halite and sylvite.

To isolate sublimates (solids precipitated directly from gas) from other types of incrustations, sublimates were collected using the silica-tube method of Le Guern and Bernard (1982). Silica-tube sublimates were collected from the high-temperature dome fumaroles in 1987 at an 870°C vent (Symonds, unpubl.) and in 1989 from vents up to 640°C (Bernard, unpubl.). The 1987 sublimates contain cristobalite, magnetite, acmite, molybdenite, bornite, halite, sylvite, pyrite, CuCl(s) and a Fe-K-Cu-S phase (Symonds, unpubl.). The 1989 sublimates are dominated by chlorides of Na, K, Cu, Zn and Pb, but also contain rare sulfides of Mo, Fe and Ni (Bernard, unpubl.).

4. Field and analytical methods

In July 1989, samples of intensely altered wall rock were collected from 640 and 375°C vents in the dome fumarole field located at the base of the spine on the 1986 dome. The 640°C fumarole is the dome vent described by Symonds et al. (1990). Hereafter, we call the 640°C vent, spine-1, and the 375°C fumarole, spine-3. We also studied fresh lava samples collected from the spine, just a few meters from the dome field, by Jürgen Kienle in 1986. These samples are representative of the 1986 dome lavas and are chemically and mineralogically similar to other 1986 eruptive products (Swanson and Kienle, 1988). The samples were analyzed by optical microscopy, X-ray diffraction (XRD), electron microprobe, scanning electron microscope (SEM), X-ray fluorescence (XRF), inductively coupled plasma-mass spectrometry (ICP–MS) and instrumental neutron activation analysis (INAA).

XRD analysis on individual alteration zones of clay size fraction (< 2 μm) separates were performed. The detector was set to count over a range of 2θ from 3 to 65°, counting for 2 seconds at each 0.03° step increment.

A microprobe analyzer was used for energy-dispersive spectroscopy (EDS) and wavelength-dispersive spectroscopy (WDS) analyses of both polished and broken surfaces of altered and fresh rock samples. Polished surfaces of the altered fumarole wall rocks were prepared for microprobe analysis by gluing pieces of altered rock onto thin-section slides with lakeside, and by impregnating the pieces with epoxy in a vacuum. The samples were then polished until all the grains were sufficiently smooth. Because this method destroys the fine and powdery incrustations from the rock surfaces, non-polished broken surfaces of the altered rocks were studied by EDS and SEM to document the various alteration mineral assemblages.

Whole-rock chemical analyses of the altered and fresh rocks were obtained at Washington State University (Hooper Laboratory) using an XRF. Rare-earth elements (REE) in the fresh andesitic lava were determined by ICP–MS at Washington State University and by INAA at Oregon State University.

5. Fresh rock petrography

The andesitic lava sample from the spine on the 1986 dome is porphyritic, weakly vesiculated and fairly dense. It is light grey in color and composed of plagioclase, pyroxene and magnetite phenocrysts in a groundmass of the same minerals. Primary hydrous minerals and quartz are absent. Anorthite-rich plagioclase, large clinopyroxene grains and magnetite typify the phenocryst assemblage. Plagioclase grains range in size from slender microlites to large phenocrysts (Fig. 2a), but no significant compositional variation exists among the different grain sizes.

Some grains of orthopyroxene are overgrown by clinopyroxene. Many calcium-rich clinopyroxene phenocrysts are up to 2 mm in size; others are included within plagioclase (Fig. 2b). Phenocrysts commonly constitute about 45–50% (by volume) of the rock.

Phenocryst rims and microphenocrysts seem to have been in mutual equilibrium, and the euhedral shapes of most crystals imply crystal–melt equilibrium as well (Johnston, 1978). The absence of hornblende and other hydrous minerals, and the abundance of plagioclase in the 1986 lava suggest that crystallization of the dome lavas occurred under low water fugacities (Yoder and Tilley, 1962; Holloway and Burnham, 1972).

6. Alteration mineralogy and zoning

Alteration assemblages were studied in samples collected from the 640°C spine-1 vent and from the 375°C spine-3 fumarole. In the spine-1 vent, distinct zoning of alteration minerals in the interiors of the wall rocks is differentiated by color bands ranging from white to grey (zone 1), pink to red (zone 2) and

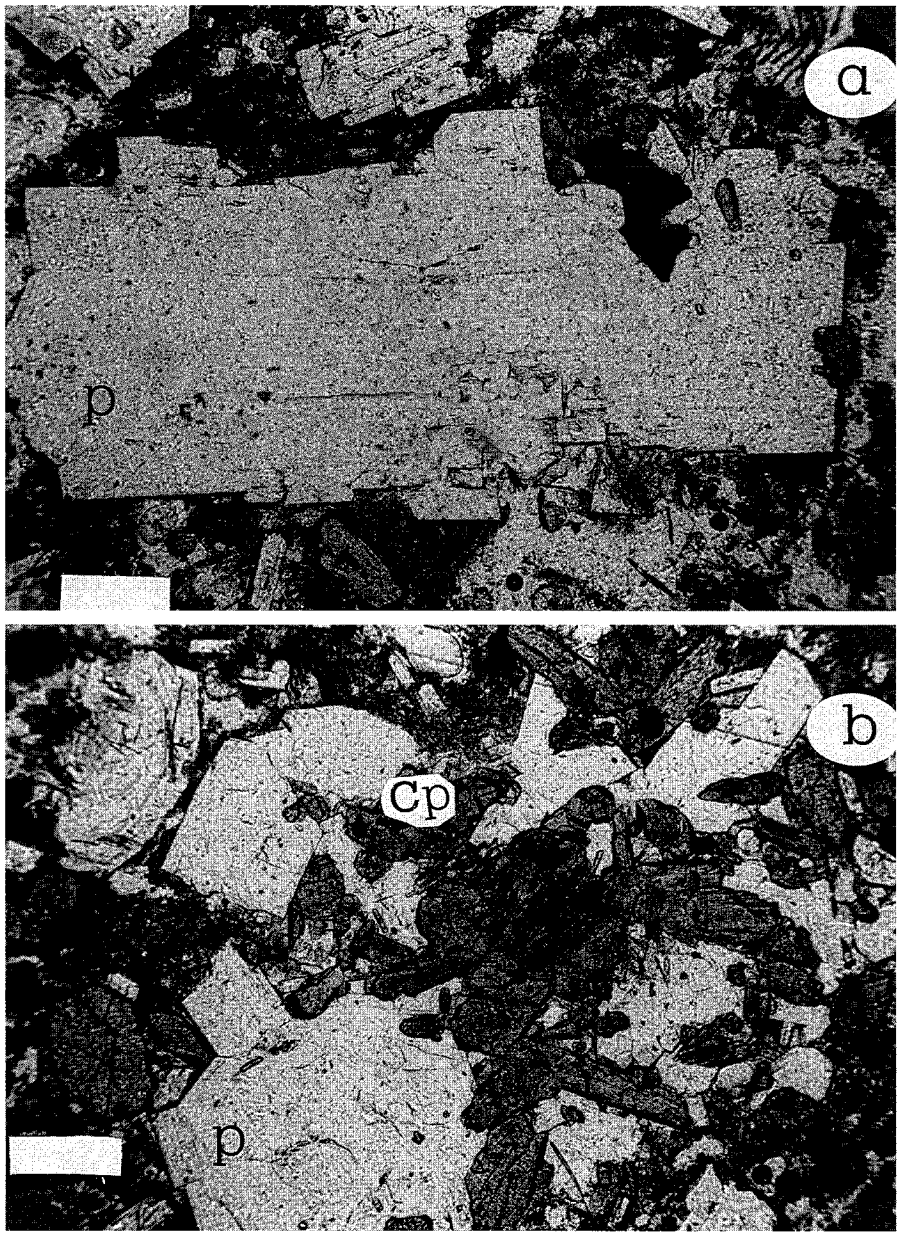

Fig. 2. Photomicrographs of the fresh andesite (MAF-1) from the spine on the 1986 lava dome. (a) Plagioclase feldspar phenocryst (*P*). (b) Phenocrysts of clinopyroxene (*Cp*) with plagioclase (*P*) and magnetite (*M*). The scale bars correspond to 0.5 mm.

dark green to green (zone 3), in order of decreasing temperature. Hereafter these zones are referred to for simplicity as the "grey", "red" and "green" zones. The color boundaries are sharp except at the green end, where the change is gradual. The width of each individual zone ranges from less than a centimeter to several centimeters. No color change was observed on the samples in the laboratory during prolonged contact with the atmosphere at room temperature.

XRD analyses of the spine-1 fumarole wall rock reveal an abundance of crystalline phases, dominantly oxides, chlorides and sulfates (Table 1). Tridymite occurs in all zones and is a dominant phase in the grey zone. Oxides, hydroxides and iron chlorides are the main constituents of the red zone. Calcium, sodium, and potassium chlorides and sulfates are the main constituents of the green zone.

EDS analyses of broken surfaces and microprobe analyses of polished surfaces of spine-1 wall rock confirm the presence of all the mineral phases identified by XRD and reveal a number of additional crystalline and amorphous phases that were not otherwise positively identified by XRD (Table 1). In the grey zone tridymite is the dominant phase (Fig. 3) with subordinate anhydrite and Al-Si phases. The red zone is composed of tridymite, an iron-chloride phase (probably molysite, $FeCl_3$), iron hydroxide and/or hematite and minor amounts of anhydrite. The iron-chloride phase occurs as small clusters of hexagonal platelets (Fig. 4a). Other minor phases identified in this zone are small cubes of halite, an amorphous Fe-Zn material (Fig. 4b) and unidentified phases containing Fe-Al-Si, Fe-Mg-Al-Cl-Si, Ca-Mg-Si and Al-Si (Fig. 4c and e). Most of the amorphous materials have dehydration cracks that run across the aggregates (Fig. 4c and d). The green zone is composed of anhydrite, halite, sylvite and a minor iron-

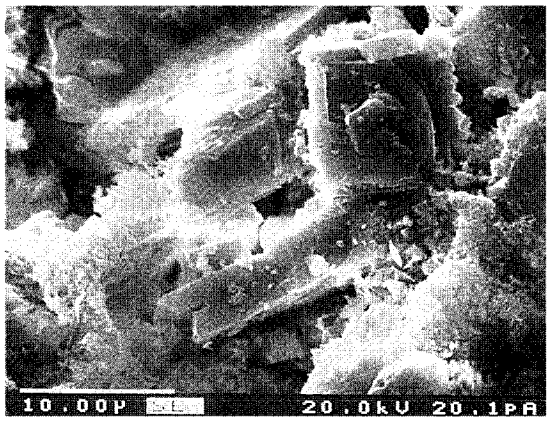

Fig. 3. SEM image from the grey zone of spine-1 showing crystalline silica (tridymite) surrounded by amorphous silica.

Table 1
Summary of alteration and assemblages in the fumarole wall rocks of Augustine volcano

Alteration sequences	Mineral and amorphous phases
Spine-1	
Zone-1 (grey zone)	Tridymite [a,b], minor anhydrite [a,b] and (Al-Si) [b]
Zone-2 (red zone)	Tridymite [a,b], hematite [a,b], hydromolysite [a], Fe-hydroxide [b], (Fe-Cl) [b] phase, and minor phases of anhydrite [b], halite [b], (Fe-Al-Si) [a], (Fe-Mg-Al-Si-Cl) [b], (Ca-Mg-Si) [b], (Al-Si) [b] and amorphous (Fe-Zn) [b] phase
Zone-3 (green zone)	Anhydrite [a,b], halite [a,b], sylvite [a,b], tridymite [a,b], and minor(Fe-Cl) [b], (K-Al-S) [b] (Na-Al-S) [b] phases and amorphous aggregates of Al-hydroxide [probably $Al(OH)_3$] [b]. Other unidentified phases include (Ca-Mg-Si) [b], (Ca-Al-Si) [b], (Ca-Mg-Fe-Si) [b], (Ca-Al) [b], (K-Fe-Ca-Ti-Al-S-Cl) [b], (Fe-Ca-K-Al-S-Cl) [b], (Ca-Fe-Si-S-Cl) [b], (K-Na-Al-Si-Cl) [b], (K-Al-Ca-Si-S-Cl) [b], (Ca-Si) [b], (Ca-K-Na-Al-Si-Cl) [b], (Ca-Mg-Cl) [b], (Ca-Br-Cl) [b], (Al-Si) [b] and (Fe-Ca-W-Cl) [b]
Spine-3	
Zone-1	Cristobalite [a,b], amorphous silica [b]
Zone-2	Cristobalite [a,b], (potash alum; K-Al-S) [a,b], (soda alum; Na-Al-S) [a,b], (aphtitalite; K-Na-S) [b], [Al-S; alunogen (?)] [b], anhydrite [a,b]

[a] Identified by XRD.
[b] Identified by EDS.

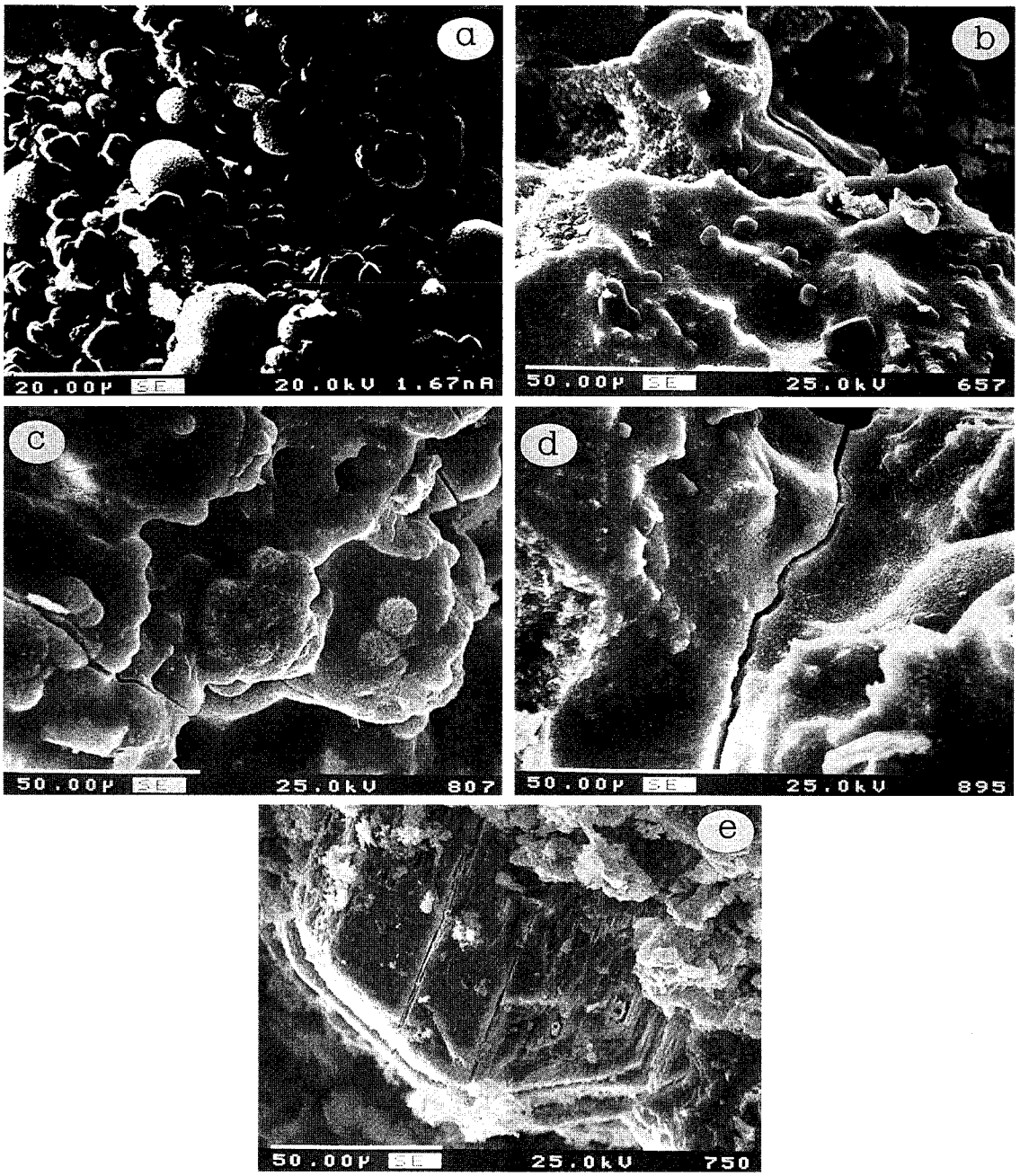

Fig. 4. SEM images of various phases from the red zone of spine-1 alteration assemblages. (a) Hexagonal platelets of Fe-Cl phase (molysite) and globules of iron oxide or iron hydroxide. (b) Amorphous Fe-Zn phase with small pellets of Fe-Mg-Al-Si-Cl phase and cubes of crystalline halite. (c) Massive Fe-Cl phase containing minor amounts of Al, Si, Mg, Na and K. It also exhibits dehydration cracks. Small pellets of Fe-Al-Si phase are also present. (d) A dehydration crack cutting across an aggregate of amorphous silica. (e) Crystalline Ca-Mg-Si phase surrounded by amorphous silica.

chloride phase (probably $FeCl_3$) accompanied by unidentified phases containing Ca-Mg-Si, Ca-Al-Si, Ca-Mg-Fe-Si, Ca-Al, Fe-Ca-K-Al-S-Cl, Ca-Fe-Si-S-Cl, K-Na-Al-Si-Cl, K-Ca-Al-Si-S-Cl, Ca-Si, K-Na-Ca-Al-Si-Cl, Ca-Mg-Cl, Ca-Br-Cl, Al-Si, Fe-Ca-W-Cl, slender crystals of K-Fe-Ca-Ti-Al-S-Cl and amorphous aggregates of Al hydroxide (Fig. 5a–h).

In the 375°C spine-3 fumarole, color zones in the altered wall rock change gradually from white to grey. These samples contain cristobalite surrounded by amorphous forms of SiO_2 (Fig. 6a). The other major alteration phases are, potash alum (Fig. 6b), soda alum, aphthitalite, Al-S (alunogen?) and minor anhydrite (Table 1).

7. Chemical composition of the fresh rock and alteration products

7.1. Major elements

Major-element compositions (Table 2) are similar to other 1986 and pre-1986 lava samples analyzed by

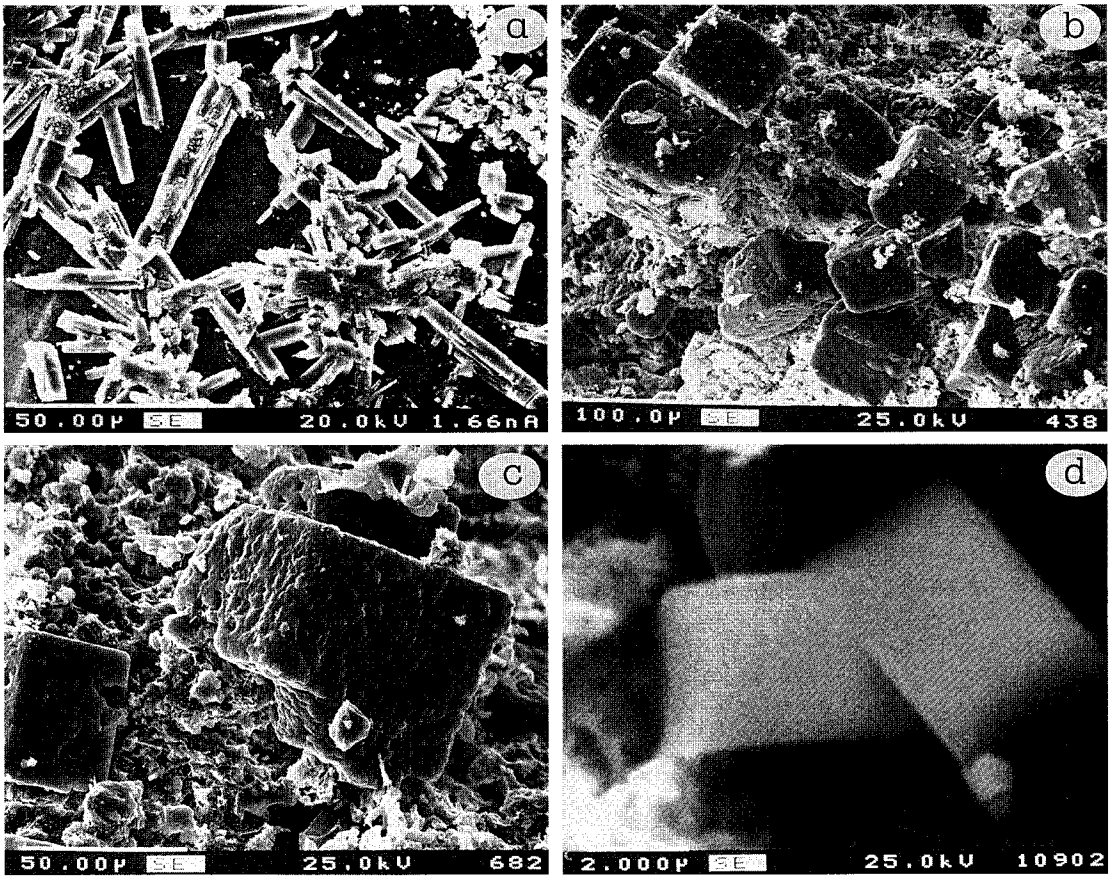

Fig. 5. SEM images of selected phases from the green zone of the spine-1 alteration assemblages. (a) Prismatic and acicular crystals of anhydrite. (b) Cubes of halite. (c) Na-K-Cl phase; Na is dominant over K. (d) Sylvite crystals with a halite blob on the right lower lobe. (e) Prismatic and tabular crystals of Ca silicate containing minor Mg, Fe, Cl and S. (f) Amorphous aluminum hydroxide with small crystals of a Ca-Al-Si-Cl phase. (g) Prismatic crystals of Ca-Mg silicate with amorphous Ca-Al-Si-S-Cl (left) and amorphous Ca-Mg-Fe-K-Al-Si-Cl (right). (h) Iron-chloride phase.

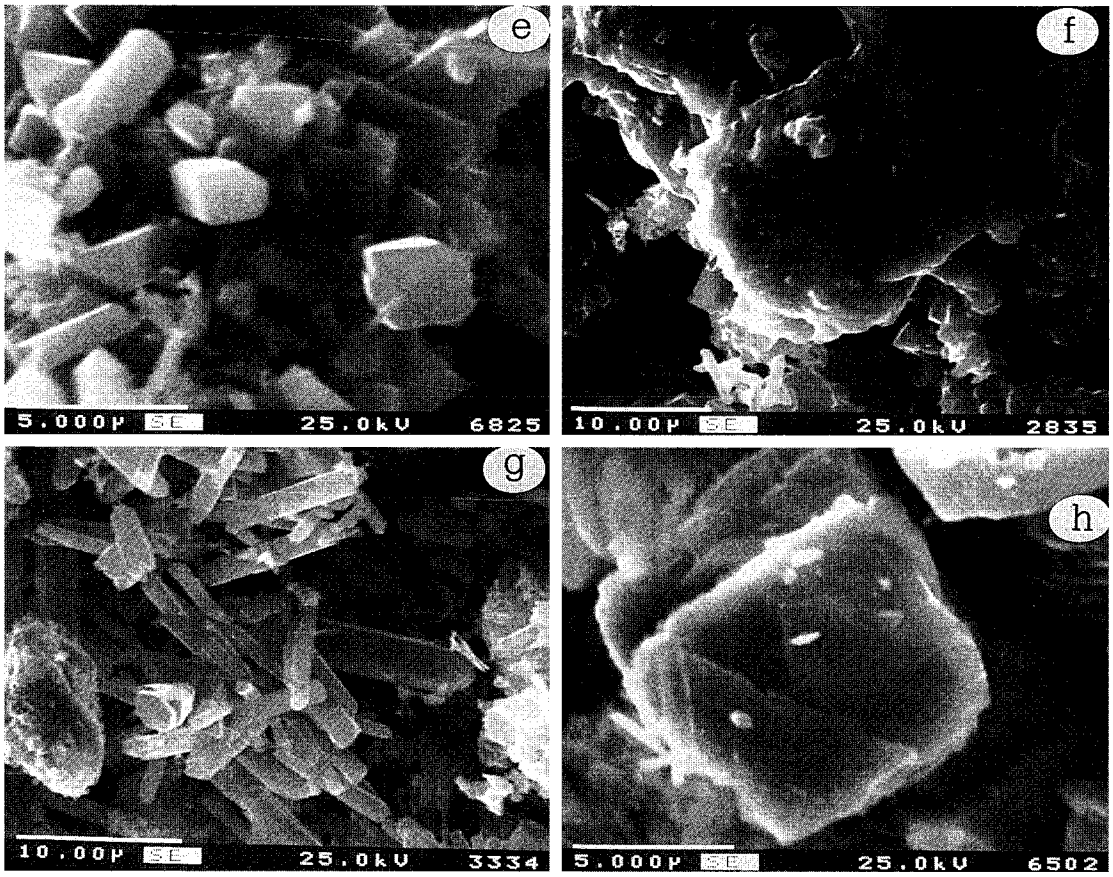

Fig. 5 (continued).

Swanson and Kienle (1988). The bulk composition of Augustine's lava is characterized by higher SiO_2 and lower FeO (total iron), CaO, Al_2O_3, MgO, TiO_2 and P_2O_5 than the western Aleutian andesitic lavas but has relatively similar values for Na_2O and K_2O. Marsh (1982) suggested that this compositional variation of Aleutian volcanic products from west to east relates to the transition of the crust from oceanic to continental.

7.2. Rare-earth element composition of the fresh lava

The contents of some trace and rare earth elements (REE) in the spine lava samples are reported in Tables 2 and 3. A chondrite-normalized graph of REE shows that the spine lavas are highly enriched in light REE such as La, Ce, Pr and Nd (Getahun, 1994). The spine-1 REE curve slopes gently up to Eu and drops sharply to Gd, and is more or less flat through the heavy rare-earth elements (HREE; Getahun, 1994). The ΣREE values for the fresh lava range from 53.88 to 55.96 ppm resembling values given by Cullers and Graf (1984) for andesites. The chondrite-normalized La/Lu ratios (2.84–2.92) and Eu/Sm ratios (0.368–0.371) are also within the andesite range (Table 4).

8. Composition of fresh and altered phenocrysts

Some of the intensely altered fumarole wall rocks contain pseudomorphs of plagioclase and pyroxene

phenocrysts with fresh cores of the remnant mineral. Using the microprobe, we analyzed such cores and the surrounding alteration rims. For comparison, we also analyzed plagioclase and pyroxene phenocrysts in unaltered lava.

8.1. Plagioclase

Analyses of phenocrysts and microlites of plagioclase in the fresh lava show that SiO_2 content ranges from 48.2 to 56.4%, averaging 53.3%. Generally the plagioclase is anorthite rich, ranging from An_{49} to An_{79}, falling mostly in the range of labradorite (Getahun, 1994).

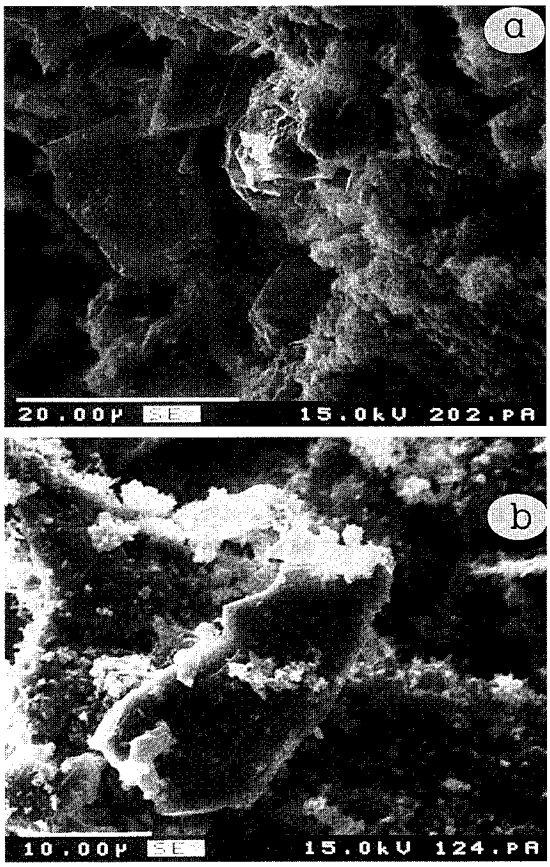

Fig. 6. SEM images of alteration assemblages from the spine-3 vent. (a) Cristobalite surrounded by amorphous silica. (b) K-Al-S (potash alum) blob surrounded by amorphous silica.

Table 2
Chemical compositions of fresh andesites collected from the spine on the 1986 lava dome [a]

	MAF-1 [b]	MAF-2 [b]
Major elements (wt.%)		
SiO_2	62.56	62.20
Al_2O_3	16.62	16.54
TiO_2	0.550	0.558
FeO [c]	5.30	5.31
MnO	0.123	0.124
CaO	6.45	6.41
MgO	3.20	3.22
K_2O	1.00	0.98
Na_2O	3.89	3.81
P_2O_5	0.042	0.045
Total	99.74	99.20
Trace elements (ppm)		
Ni	21	21
Cr	44	49
Sc	14	14
V	131	113
Ba	423	433
Rb	21	20
Sr	312	311
Zr	113	37
Y	17	17
Nb	4.0	7.5
Ga	16	15
Cu	23	17
Zn	54	54
Pb	1	0
Co	57.69	nd
As	< 5.70	nd
Hf	3.14	nd
Ta	2.07	nd
W	171.30	nd
Th	2.3	nd
U	0.94	nd

Major elements are not normalized to 100%; nd = not determined.
[a] Analyses for Co, Hf, Ta, W, Th and U are determined by INAA and the rest by XRF.
[b] Samples collected by Jürgen Kienle.
[c] Total Fe is expressed as FeO.

The compositions of remnant cores of altered plagioclase phenocrysts range from An_{54} to An_{61} (Table 4). These are surrounded by alteration rims enriched in silica (92–95% SiO_2). Al_2O_3, CaO, Na_2O and K_2O are extremely depleted from the altered plagioclase, leaving behind silica (Fig. 7a). The alteration rims are also enriched in chloride,

sulfur and fluoride, owing to the incorporation of these elements from the volcanic gas during gas–rock reaction.

8.2. Pyroxene

The major-element analyses of pyroxene phenocrysts in the fresh lava reveal that the calcium-rich clinopyroxenes range from En_{44} to En_{43} falling in the fields of augite and salite (Getahun, 1994). One analysed orthopyroxene has a composition of En_{68} and falls in the range of hypersthene (Getahun, 1994). Pyroxene pseudomorph analyses in the altered fumarole wall rock (Table 5; Fig. 7b) show that fresh remnant cores of pyroxenes are surrounded by alteration products comprised dominantly of SiO_2 (up to 95%) and that FeO, MgO and CaO are strongly depleted. The rims are also enriched with Cl^-, S and F^-.

9. Major- and trace-element compositions of the altered rocks

The chemical compositions of the altered fumarole wall rocks are given in Tables 6, 7 and 8. The sums of all the major-element oxides in the altered rock are significantly less than 100% because these samples contain large amounts of volatiles. The grey zone of spine-1 (MAD-1–MAD-4) is characterized by a high silica content ranging from 70 to 80%. The red zone (MAD-5–MAD-6) contains relatively large amounts of total iron, while the green zone (MAD-7–MAD-8) contains significantly elevated amounts of Ca, K and Na. The alteration products from spine-3 (Table 8) are extremely silica rich (89–93% SiO_2).

The mobility of major, trace and REE elements during gas–rock reaction and development of fumarole wall rock alteration mineral assemblages were investigated further by computing the changes in element concentrations relative to the Augustine fresh rock. The assumption for this computation is that the volume of the fresh rock that was subjected to alteration remained constant during the reaction pro-

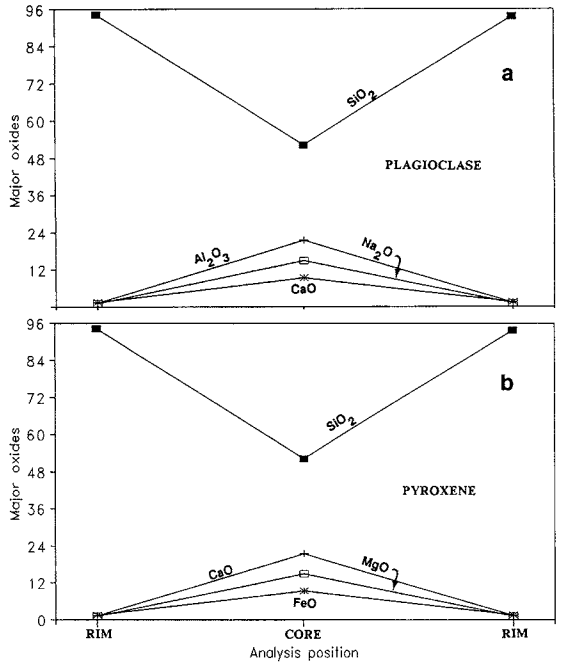

Fig. 7. Variation diagrams showing the across-grain composition of a typical altered plagioclase feldspar (a) and pyroxene (b). The remnant cores represent the unaltered composition of fresh-rock feldspar and pyroxene.

Table 3
REE compositions (ppm) of fresh andesite collected from the spine on the 1986 lava dome

	MAF-1 [a]	MAF-1 [b]	MAF-2 [b]
La	9.00	9.60	9.23
Ce	20.70	18.65	17.87
Pr	nd	2.30	2.20
Nd	10.20	10.04	9.54
Sm	2.49	2.64	2.58
Eu	0.90	0.98	0.95
Gd	nd	2.64	2.58
Tb	0.42	0.50	0.48
Dy	nd	3.15	3.08
Ho	nd	0.68	0.67
Er	nd	2.08	2.03
Tm	nd	0.30	0.30
Yb	1.94	2.06	2.03
Lu	0.32	0.34	0.34
ΣLREE	43.29	43.23	42.46
ΣHREE	2.68	12.73	12.46
ΣREE	45.97	55.96	54.92

nd = not determined.
[a] Analysis done by INAA.
[b] Analysis done by ICP–MS.

cesses. This assumption is supported by the observation that most of the phenocryst pseudomorph textures in the altered rock are dimensionally similar to those in the fresh rock. The weight-basis chemical compositions of the fresh and altered products were converted to volume-basis compositions by multiplying by the rock densities. The resulting values for altered rocks were subtracted from those for fresh rock and the differences are shown graphically in Figs. 8 and 9.

9.1. Spine-1 fumarole (640°C)

On the basis of their color and mineralogical assemblages, the altered rocks of spine-1 were grouped into the grey, red and green zones (see above). The discussion of the mobility of the elements across the alteration zones refers to these three zones.

9.1.1. Major elements

The grey zone, characterized by abundant tridymite, is enriched distinctly in SiO_2 and depleted in all other major oxides (Al_2O_3, TiO_2, FeO, MnO, CaO, MgO, Na_2O and P_2O_5) except K_2O (Fig. 8a). Note that because all of the chemical compositions are expressed on a volume basis, the enrichment in SiO_2 and depletion in other major-element oxides indicates a true transfer of SiO_2 into the grey zone and a true removal of the other oxides from the grey zone. The red zone, characterized by significant amounts of iron chlorides and iron oxides, has gains in FeO, TiO_2, MnO, MgO and P_2O_5 and losses in K_2O, Na_2O and Al_2O_3 (Fig. 8a). The green zone, characterized by abundant anhydrite, halite and sylvite, is enriched in CaO, Na_2O, K_2O, P_2O_5 and TiO_2, and depleted in SiO_2, Al_2O_3, FeO and MnO (Fig. 8a). MgO in the green zone is near the fresh-rock value where anhydrite is dominant but it is depleted where halite and sylvite are dominant (Fig. 8a).

Al_2O_3 is depleted in all alteration zones but approaches the fresh rock value in the red zone (Fig. 8a). The retention of Al in the red zone is caused by the formation of aluminum-bearing silicates (Table 1).

9.1.2. Trace elements

All the trace elements given in Fig. 8b and c, except Rb, Cu, Zn and Pb, exhibit depletion in the grey zone. The gains in Cu, Zn and Pb are also minimal compared to the other two zones. All or part of the red zone is enriched in Ni, Cr, Sc, V, Zr, Y, Cu, Zn and Pb and it shows near-fresh-rock values for Ba, Rb, Sr, Nb and Ga (Fig. 8b and c). The green zone gained Sr, Ba and Ga in the inner part where anhydrite is dominant but lost these elements in the outer part where halite and sylvite are dominant.

Table 4
Electron probe analyses of core remnants and alteration rims of plagioclase feldspars from the spine-1 fumarole wall rocks

Grain no.:	1		2		3		4		
Site:	Core	Rim	Core	Rim	Core	Rim	Rim	Core	Rim
SiO_2	52.72	95.07	53.89	91.97	55.19	93.38	93.40	54.12	92.68
Al_2O_3	29.70	1.25	28.83	2.86	28.13	2.05	1.92	28.77	2.13
CaO	12.74	0.72	12.02	1.23	11.14	1.45	1.18	11.75	1.21
FeO	0.48	0.86	0.54	0.79	0.45	0.89	0.82	0.47	0.95
Na_2O	4.20	0.55	4.50	0.72	5.13	0.76	0.70	4.73	0.72
K_2O	0.07	0.00	0.12	0.04	0.12	0.09	0.03	0.10	0.04
Total	99.91	98.45	99.90	97.61	100.16	98.62	98.05	99.94	97.69
Ab	37.15		40.08		45.11			38.41	
Or	0.43		0.68		0.70			0.61	
An	62.42		59.24		54.19			60.98	

Table 5
Electron probe analyses of core remnants and alteration rims of pyroxenes from altered spine-1 fumarole wall rocks

Grain no.:	1		2		3		4		
Site:	Core	Rim	Core	Rim	Core	Rim	Rim	Core	Rim
SiO_2	51.81	94.95	52.45	91.56	52.56	93.25	94.10	52.21	93.67
TiO_2	0.26	0.02	0.06	0.04	0.25	0.03	0.02	0.22	0.03
Al_2O_3	1.42	0.23	0.83	0.52	1.32	0.38	0.28	1.35	0.29
Fe_2O_3	3.26	0.29	2.81	0.19	2.33	0.24	0.28	2.63	0.27
MgO	14.85	1.11	20.49	1.08	14.96	1.10	1.15	14.87	1.14
CaO	21.33	1.32	1.09	0.05	21.51	1.21	1.27	21.46	1.28
MnO	0.45	0.12	0.96	0.01	0.47	0.07	0.07	0.45	0.09
FeO	6.15	0.61	21.22	6.11	6.80	1.74	1.20	6.63	1.19
Na_2O	0.35	0.02	0.04	0.01	0.33	0.04	0.03	0.34	0.06
K_2O	0.00	0.00	0.02	0.00	0.00	0.00	0.00	0.00	0.00
Total	99.88	98.67	99.97	99.57	100.53	98.06	98.33	100.16	98.02
Wo	45.24		2.55		44.79			44.99	
En	43.81		47.87		43.36			43.39	
Fs	10.95		49.58		11.85			11.62	

Table 6
Chemical compositions of the altered spine-1 rocks

	Grey zone			Red zone		Green zone	
	MAD-1	MAD-2	MAD-4	MAD-5	MAD-6	MAD-7	MAD-8
Major elements (wt.%)							
SiO_2	79.54	69.88	80.37	60.70	59.64	49.47	54.34
Al_2O_3	2.89	7.11	5.71	11.35	13.88	10.61	10.47
TiO_2	0.297	0.335	0.381	1.070	0.899	0.798	0.626
FeO [a]	2.09	3.86	2.46	4.92	6.62	4.31	4.27
MnO	0.053	0.080	0.067	0.113	0.124	0.106	0.072
CaO	0.96	1.92	1.39	7.59	6.70	12.51	6.25
MgO	1.41	2.31	1.90	3.64	4.11	3.30	2.23
K_2O	0.89	1.21	0.75	0.51	0.69	2.58	4.55
Na_2O	0.50	1.11	0.81	2.13	2.59	4.83	8.07
P_2O_5	0.028	0.082	0.085	0.093	0.076	0.091	0.042
Total	88.66	87.90	93.89	92.11	95.35	88.59	90.97
Trace elements (ppm)							
Ni	13	17	15	19	22	17	14
Cr	21	33	18	58	74	52	50
Sc	3	5	4	34	24	23	13
V	9	102	40	114	178	334	+583
Ba	123	313	170	453	391	471	258
Rb	123	126	100	34	35	220	225
Sr	28	81	57	297	257	560	259
Zr	54	85	96	120	110	122	76
Y	6	12	13	22	20	28	20
Nb	8.3	3.4	7.4	4.9	6.2	1.8	5.8
Ga	1	8	7	13	15	17	10
Cu	127	92	113	82	+154	+350	+296
Zn	106	113	+253	+153	+497	+519	+643
Pb	32	+78	+1165	+569	+778	+257	20

Major elements are not normalized to 100%; + = values > 120% of highest standard.
[a] Total Fe is expressed as FeO.

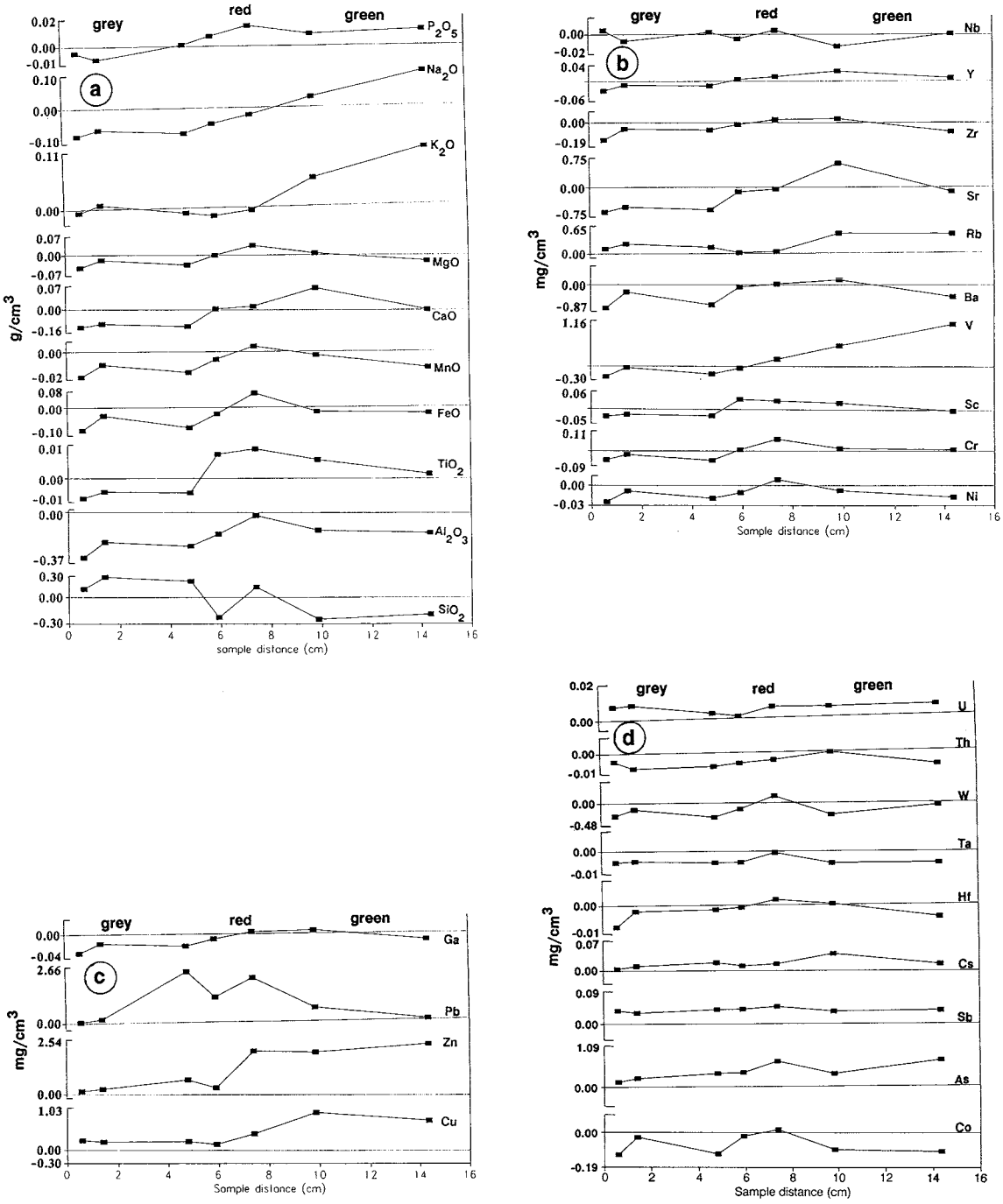

Fig. 8. Gains and losses of major oxides (a) and some trace elements and REEs (b–e) in the alteration zones of spine-1 (640°C). The fresh-rock value is represented by the zero-line.

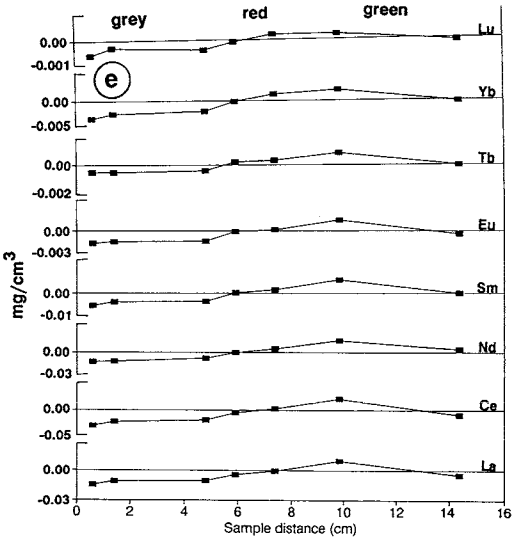

Fig. 8 (continued).

Otherwise, the green zone is enriched in V, Y, Cu, Zn and Pb (Fig. 8b and c) but depleted in Ni and Nb. The enrichment of Sr and Ba in the inner green zone and their depletion in the outer green zone, the same trend as observed for CaO (Fig. 8a), indicate a close geochemical relationship among Sr, Ba and Ca.

As, Sb, Cs and U are enriched in all zones. Co, Hf and W are removed from the grey and green zones, but slightly enriched in the red zone (Fig. 8d). Ta and Th are depleted in all zones, but Ta shows near-fresh-rock values in the red zone and Th approaches fresh rock values at the inner part of the green zone, where anhydrite is the dominant component (Fig. 8d).

9.1.3. Rare-earth elements

The average ΣREE of the alteration zones ranges from 24 ppm in the grey zone to 47 ppm in the red zone to 78 ppm in the green zone. The highest ΣREE value (114 ppm) is from the inner part of the green zone where anhydrite is the major constituent. The ΣLREE and the ΣHREE are also highest in the green zone followed by the red and grey zones (Table 7). The grey zone is characterized by a low ΣREE (24 ppm), low ΣLREE (22 ppm) and low ΣHREE (1.4 ppm) compared to the fresh rock (Table 3). The red zone is represented by near-fresh-rock values of ΣREE (47 ppm) and ΣLREE (44 ppm), but slightly higher ΣHREE (3.1 ppm) than the fresh rock. The average of the green zone samples exhibits higher ΣREE (78 ppm), ΣLREE (75 ppm) and ΣHREE (3.4 ppm) than Augustine fresh rock (Table 3).

The REE exhibit similar distribution patterns in all three alteration zones. Both LREE and HREE are depleted from the grey zone. The LREE have near-fresh-rock values in the red zone and are enriched in the inner part of the green zone (Fig. 8e). The HREE are gained in both the red and green zones.

One striking feature of Fig. 8 is the parallelism of the curves for the following elemental groups: FeO-Ni-Cr-MnO-MgO, TiO_2-Sc, K_2O-Na_2O-V and CaO-Sr-Ba-Ga. The distributions of nearly all the REE also resemble the pattern of calcium. These striking similarities in the distribution patterns of these elements indicate their chemical association and coherent fractionation during rock alteration and mineral precipitation.

9.2. Spine-3 fumarole (375°C)

Alteration products from the spine-3 fumarole contain abundant cristobalite (see above). Alteration color bands in the spine-3 vent change gradually from white near the vent to grey away from the vent. The bulk chemical compositions of spine-3 alteration products are given in Table 8. The gains and losses of major oxides and trace element of these zones are plotted with reference to unaltered rock in Fig. 9.

9.2.1. Major elements

Compared to the 1986 lava (Table 2), the spine-3 alteration zones exhibit enrichment in SiO_2 (Fig. 9). All other elements, including Al_2O_3, TiO_2, FeO, MnO, CaO, MgO, K_2O, Na_2O and P_2O_5 are strongly depleted in the alteration products (Fig. 9). The depletion of these elements is tied to the destruction of primary minerals from the rock.

9.2.2. Trace elements

All trace elements except Cu, Pb and to some degree La and Ce exhibit depletions compared to the

1986 lava (Getahun, 1994). Cu and Pb show gains in both the white and grey zones, while La and Cs are enriched in the grey zone (Getahun, 1994). All primary minerals in the spine-3 altered rock are disintegrated and replaced by secondary minerals, dominantly cristobalite and minor sulfates.

Retention of trace elements in altered rocks is facilitated by preservation of primary minerals that contain them and by the formation of secondary alteration minerals that incorporated these elements into their structures (e.g., Humphris, 1984). In the spine-3 samples, the primary igneous minerals were completely destroyed by the alteration process which eliminated the hosts for many trace elements.

10. Thermochemical modeling

To understand better fumarole wall rock alteration processes at Augustine, we used the thermochemical modeling program, GASWORKS, to model the complex geochemical processes occurring around these fumaroles. GASWORKS (Symonds and Reed, 1993) calculates heterogenous equilibria among gases, minerals and liquids during the processes of cooling or heating, pressure change, gas–gas mixing and gas–rock reaction. The program models gas–mineral–liquid equilibria in systems of up to 42 elements using the basic formulation of equilibrium calculations for aqueous–mineral–gas systems of Reed (1982) modified for gaseous systems (Symonds and Reed (1993). The calculations use the thermodynamic data base, GASTHERM (Symonds and Reed, 1993).

The numerical modeling is constrained with natural samples. The simulations require the complete gas composition, including trace elements, as well as the bulk composition of the fresh rock and the temperatures and pressures of the alteration zones. Gases and condensates (condensed volcanic gas analyzed for metals) were collected from the spine-1 vent in the dome fumarole field in 1987 and 1989 (Symonds et al., 1990; Symonds, unpubl.). Specifi-

Table 7
Some trace and rare earth element compositions (ppm) of altered spine-1 rocks. The analysis is done using INAA

	Grey zone			Red zone		Green zone	
	MAD-1	MAD-2	MAD-4	MAD-5	MAD-6	MAD-7	MAD-8
Co	5.17	45.14	7.55	57.21	58.58	16.48	12.78
As	118.28	94.90	171.10	181.70	250.80	138.80	288.10
Sb	20.30	13.97	20.87	21.42	19.14	15.40	16.92
Cs	2.85	4.66	9.36	6.16	5.96	16.00	16.91
La	3.50	4.30	5.40	8.20	7.70	12.40	6.90
Ce	8.60	10.20	14.00	21.30	19.50	29.30	16.60
Nd	4.70	4.20	7.30	11.80	11.30	17.70	12.60
Sm	0.92	1.26	1.52	2.87	2.59	4.13	2.44
Eu	0.27	0.27	0.37	0.98	0.86	1.40	0.74
Tb	0.59	0.86	1.28	0.55	0.46	0.70	0.43
Yb	0.59	0.86	1.28	2.19	2.22	2.68	1.84
Lu	0.11	0.20	0.20	0.34	0.37	0.40	0.28
Hf	1.79	2.78	3.23	3.39	3.19	3.05	2.16
Ta	1.79	2.78	3.23	0.45	1.65	0.20	0.30
W	59.10	107.00	43.80	131.10	205.40	54.10	143.70
Th	0.80	1.10	1.40	1.70	1.50	2.10	1.20
U	< 5.10	< 4.50	< 2.60	< 1.80	< 3.30	< 3.30	< 3.60
ΣLREE	17.99	20.23	28.59	45.15	41.95	109.93	39.28
ΣHREE	1.18	1.28	1.75	3.08	3.05	3.78	2.55
ΣREE	19.17	21.51	30.34	48.23	45.00	113.71	41.83

Table 8
Chemical compositions of the altered spine-3 rocks

	MAM-1 White	MAM-2 Grey	MAM-3 White	MAM-4 Grey
Major elements (wt.%)				
SiO_2	94.16	91.63	93.36	88.86
Al_2O_3	1.26	1.39	1.66	1.80
TiO_2	0.208	0.175	0.323	0.217
FeO [a]	0.19	0.20	0.68	0.43
MnO	0.007	0.008	0.012	0.009
CaO	0.18	0.19	0.25	0.17
MgO	0.04	0.04	0.22	0.14
K_2O	0.17	0.22	0.26	0.25
Na_2O	0.21	0.33	0.25	0.32
P_2O_5	0.012	0.012	0.021	0.020
Total	96.44	94.20	97.04	92.22
Trace elements (ppm)				
Ni	9	9	10	11
Cr	7	1	5	6
Sc	7	0	0	1
V	7	5	10	10
Ba	27	29	45	10
Rb	9	11	9	9
Sr	9	10	12	9
Zr	37	48	44	46
Y	0	1	2	2
Nb	2.7	2.1	4.3	4.9
Ga	1	1	3	4
Cu	53	47	50	91
Zn	4	14	16	61
Pb	13	18	30	61
La	0	9	0	6
Ce	13	27	18	34
Th	0	1	0	1

Major elements are not normalized to 100%.
[a] Total Fe is expressed as FeO.

cally, we used the dome-3 sample (Symonds et al., 1990) to represent the 1987 spine-1 gases and an average of five samples to represent the 1989 gases (Symonds, unpubl.). These are restored equilibrium gas compositions. Restored compositions are based on relatively complete analyses and assumption that the exhaled high-temperature gases initially approached a state of chemical equilibrium, which is consistent with all past work (Gerlach, 1980a,b). We believe that the restored compositions are much more reliable than the raw gas analyses, which suffer from several sampling problems as discussed below. First, we tested whether the 1987 and 1989 gases were equilibrium mixtures using a thermodynamic procedure (Symonds et al., 1994). The results showed that both the 1987 and 1989 analyses suffer from disequilibrium oxidation of reduced-gas species; the 1987 gases also suffer from disequilibrium H_2O loss (Symonds et al., 1994). Then, we restored the samples to initial equilibrium state, by removing thermodynamically the disequilibrium effects. The restored 1989 gases are much richer in H_2O than the 1987 gases. This probably reflects a much larger meteoric vapor component in the 1989 gases, as expected with increasing time after the 1986 eruption. Trace-element contents in the 1987 and 1989 spine-1 gases were estimated using condensates collected contemporaneously from the same vent. The complete gas compositions, including trace elements, are reported in Table 9. The bulk compositions of the fresh lavas and altered wall rocks are reported in Tables 2, 6 and 8.

The purpose of this numerical simulation is to understand the processes that caused the formation

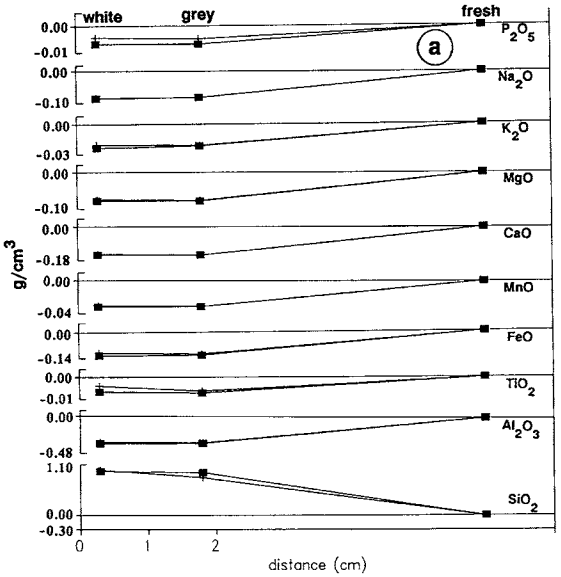

Fig. 9. Gains and losses of major oxides in the alteration zones of spine-3 (375°C). The fresh-rock value is represented by the zero-line. The distance from the grey zone to the fresh rock is unknown so we plot it for comparison purposes only.

Table 9
Reconstructed Augustine gas compositions including major gas species and trace elements for the restored samples collected from the spine-1 vent. Data are from Symonds et al. (1990) and Symonds (unpubl.)

	1987 Dome-3	1989 gas [a]
Major gas species (mol%)		
H_2O	83.91	96.84
HCl	6.04	0.50
SO_2	5.72	0.26
CO_2	2.40	1.48
H_2S	1.00	0.33
H_2	0.63	0.55
S_2	0.20	nd
HF	0.086	0.029
CO	0.020	0.0065
Trace elements (mol%)		
Si	0.83E−02	0.63E−03
B	0.45E−02	0.33E−02
Na	0.14E−02	0.76E−03
K	0.87E−03	0.45E−03
Br	0.68E−03	nd
Fe	0.16E−03	0.35E−04
As	0.99E−04	0.64E−04
Zn	0.64E−04	0.43E−04
Ca	0.46E−04	0.12E−03
Al	0.27E−04	0.26E−04
Pb	0.24E−04	0.23E−04
Mo	0.18E−04	0.78E−06
Cu	0.69E−05	0.26E−05
Li	0.67E−05	< 0.26E−05
Mg	0.48E−05	0.12E−04
Sb	0.38E−05	0.19E−05
Cd	0.21E−05	0.21E−05
Mn	0.17E−05	0.84E−06
Ti	0.65E−06	0.41E−05
Bi	0.24E−06	< 0.85E−07
Ni	0.22E−06	0.42E−04
Zr	0.17E−06	nd
V	0.15E−06	< 0.35E−06
Cr	0.12E−06	0.17E−05
Sr	0.53E−07	0.18E−06
Ba	0.28E−07	nd

nd = not determined.
[a] Average of five samples.

of the zoned incrustations and pneumatolytic rock alteration that commonly border volcanic fumarole vents, focusing particularly on Mount St. Augustine. The color banding displayed by altered fumarole wall rocks, reflects complex interactions among the cooling volcanic gases, the wall rocks and the atmosphere (e.g., Stoiber and Rose, 1974; Getahun et al., 1992). The responsible physical and geochemical processes can be tested using thermochemical modeling (Symonds et al., 1987, 1992; Le Guern, 1988; Quisefit, 1988; Quisefit et al., 1989; Getahun et al., 1992; Symonds and Reed, 1993).

The geologic framework of the alteration process is shown in Fig. 10 and is based on the assumption that the alteration bands in the 1989 spine-1 and spine-3 vents formed over a period of up to three years starting when the vents formed in 1986 by a combination of gas–rock reactions, mineral precipitation from gas cooling and mixing of volcanic gas with air. In this study, we explore the alteration processes with the following calculations: (1) reaction of the 1989 gases with the wall rock at 640 and 375°C to simulate ongoing gas–rock alteration in the spine-1 and spine-3 vents; (2) repeat the 640°C calculation in (1) using the 1987 gases to model alteration that might have occurred before 1989; (3) cooling of the 1987 gases from 870°C (their equilibrium temperature) to 100°C with and without mineral fractionation to model the sublimates that precipi-

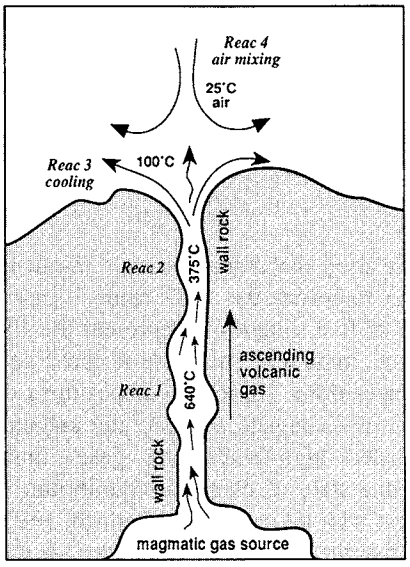

Fig. 10. Schematic representation of a fumarole showing positions of reaction calculations as described in text.

tated from the gas before 1989; (4) repeat (3) using the 1989 gas composition and start at 757°C (the equilibrium temperature of the 1989 gases) to simulate the ongoing sublimate precipitation; (5) mix air with the 1987 and 1989 gases to predict the solids that form by volcanic gas–air reaction.

11. Volcanic gas–rock reaction

This calculation involves the stepwise titration of the fresh Augustine andesite into the 1987 and 1989 spine-1 gases (Table 9) at a fixed temperature, pressure and oxygen fugacity (f_{O_2}). The simulations were carried out at temperatures of 640 and 375°C and 1 atmosphere.

11.1. Gas–rock reaction at 640°C

The starting gas compositions for these calculations were obtained by cooling the restored 1987 and 1989 gases (Table 9) from their equilibrium temperatures of 870 and 757°C, respectively, to 640°C. Then, the cooled gases were separated from the > 640°C mineral precipitates and reacted with fresh Augustine andesite (Table 2). The log f_{O_2} was fixed at −16.66 and −16.80 for the 1987 and 1989 gases, respectively. These 640°C f_{O_2} values were obtained

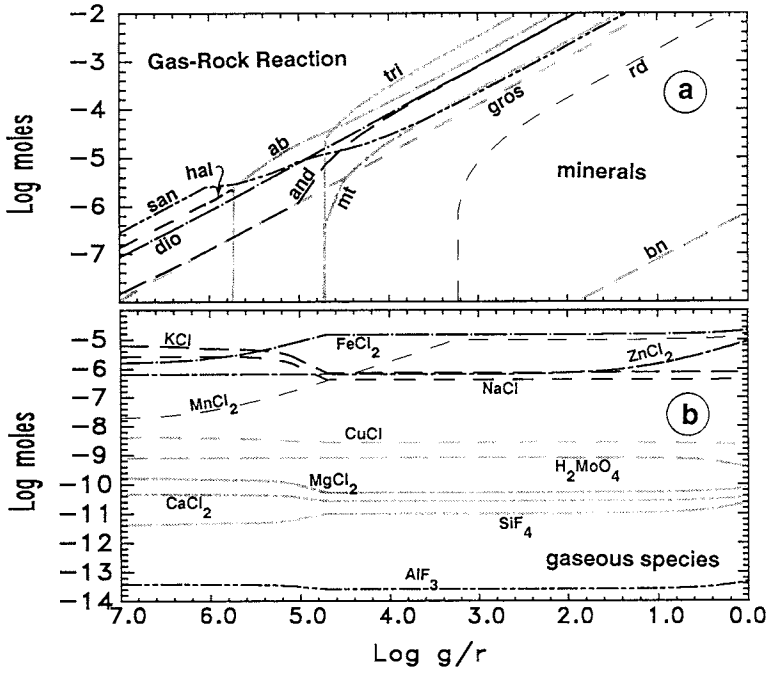

Fig. 11. Reaction of the 1987 dome-3 gas with fresh 1986 andesitic lava at 640°C. The abscissa shows the log gas/rock ratios. (a) Quantities of major alteration minerals formed. (b) log mole concentrations of dominant gaseous species. Mineral abbreviations used here and in Fig. 12Fig. 13Fig. 14Fig. 15Fig. 16Fig. 17Fig. 18 are as follows: *ab* = albite; *an* = anorthite; *ang* = anglesite ($PbSO_4$); *and* = andalusite; *anh* = anhydrite; *arc* = arcanite; *bn* = bornite; *cc* = chalcocite; *ccy* = chalcocyanite; *cor* = corundum; *cord* = cordierite; *cotn* = cotunnite ($PbCl_2$); *cv* = covellite; *dio* = diopside; *f(O₂)* = fugacity of oxygen; *gn* = galena; *gros* = grossularite; *hal* = halite; *heaz* = heazlewoodite; *hed* = hedenbergite; *hem* = hematite; *mb* = molybdenite; *mbd* = molybdite; *mic* = microcline; *mill* = millerite; *mt* = magnetite; *orp* = orpiment (As_2S_3); *py* = pyrite; *qz* = quartz; *rd* = rhodonite; *san* = sanidine; *sl* = sphalerite; *S(L)* = liquid sulfur; *S(M)* = monoclinic sulfur; *S(O)* = orthorhombic sulfur; *syl* = sylvite; *tep* = tephroite; *then* = thenardite; *tr* = tremolite; *tri* = tridymite; *wur* = wurtzite (ZnS); *wol* = wollastonite; *zin* = zinkosite; *zoi* = zoisite.

from the equilibrium cooling calculation of the 1987 and 1989 gases at 1 atmosphere.

11.1.1. The 1987 gas–rock reaction at 640°C

This gas–rock reaction produces a large assemblage of silicates plus a few oxides and sulfides. Sanidine, diopside, halite, andalusite and grossularite start to form at large log gas/rock (lg/r) ratios. Albite replaces halite at lg/r ratio of 6, and, as the g/r ratio decreases further, tridymite and magnetite precipitate (Fig. 11a). Thereafter, tridymite becomes the dominant mineral in the system. (The use of temporal terms (e.g., thereafter, early) is for convenience in discussion only.) At a lg/r ratio of 3.2 rhodonite precipitates fixing the rhodonite–quartz–$MnCl_2$ buffer and thereby holding constant the concentration of $MnCl_2$ (Fig. 11b).

11.1.2. The 1989 gas–rock reaction at 640°C

This titration produces a mineral assemblage of silicates, oxides and sulfides (Fig. 12). At high lg/r ratios (> 4.8) albite dominates the precipitated assemblage. Tridymite starts forming at lg/r ratio of 5 and soon becomes the principal alteration mineral followed by albite (Fig. 12a). Sulfides include early bornite and late chalcocite, molybdenite and sphalerite.

In contrast to the 640°C 1987 gas–rock reaction, the 1989 gas–rock reaction produces hercynite ($FeAl_2O_4$), zoisite, chalcocite and sphalerite and early albite in place of early halite. Otherwise, both results contain a final equilibrium assemblage dominated by tridymite, albite, diopside, sanidine, and other silicates and minor oxides.

11.2. The 1989 gas–rock reaction at 375°C

The starting gas composition for this calculation is obtained by cooling the restored 1989 gas (Table 9) from its equilibrium temperature of 757 to 375°C.

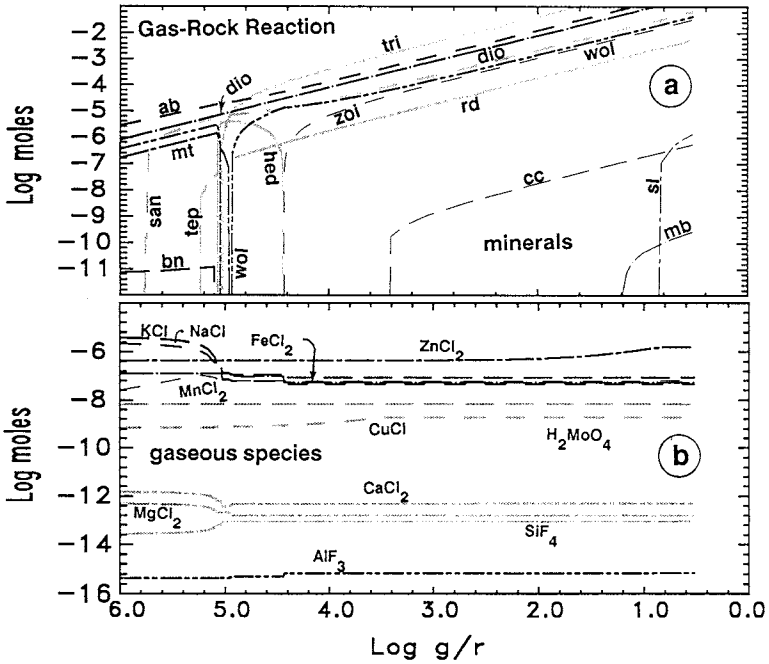

Fig. 12. Reaction of the 1989 spine-1 gas with fresh 1986 andesitc lava at 640°C. The abscissa shows the log gas/rock ratios. (a) Quantities of major alteration minerals formed (for mineral abbreviations see Fig. 11). (b) Log mole concentrations of dominant gaseous species.

Then, the cooled gas was separated from the > 375°C mineral precipitates and reacted with fresh Augustine andesite (Table 2).

This reaction yields silicates, oxides, sulfides and sulfates (Fig. 13). Quartz is the dominant alteration mineral throughout the 375°C gas–rock reaction. Albite and anhydrite are the main secondary minerals, but the proportion of anhydrite decreases as anorthite starts to precipitate at a lg/r ratio of 2.3. Halite precipitates at a lg/r ratio of 2.24 and continues to form until the calculation is terminated (Fig. 13a).

12. Comparison of computed results with observed alteration assemblages

To evaluate the contribution of gas–rock reactions in producing part of the Augustine fumarole alteration assemblages, we compare the calculated minerals to those observed. Such comparisons also help evaluate the input assumptions and thermochemical data used for the numerical simulations. The silicates that precipitate in the numerical gas–rock titrations resemble many of the silicates in the altered fumarole rocks (Table 1). For example, the

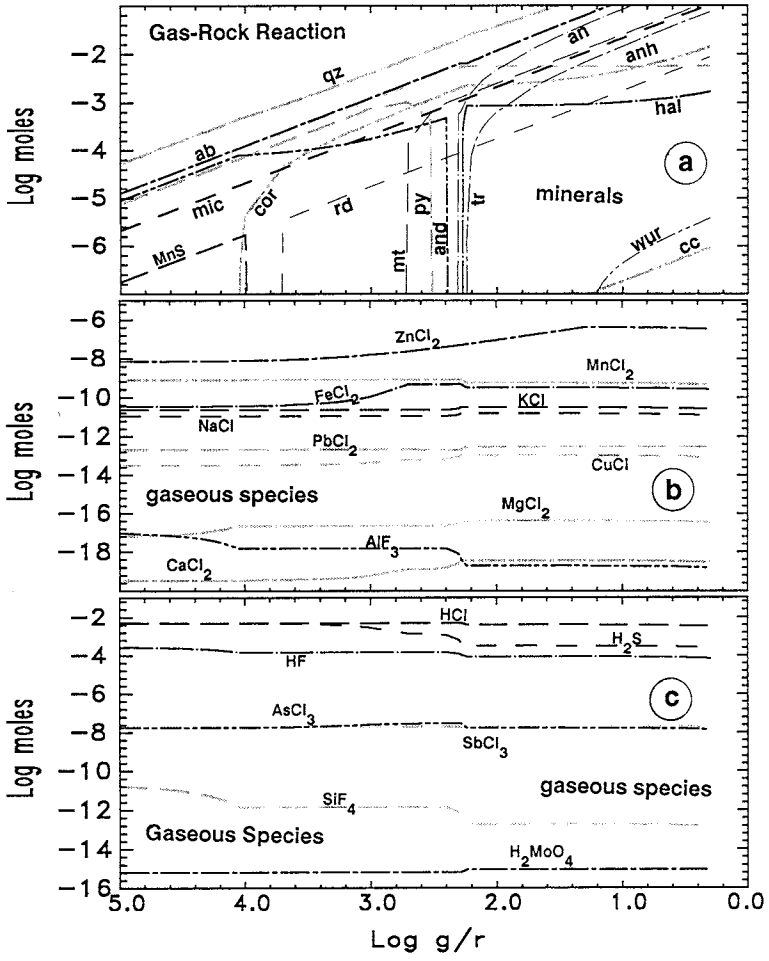

Fig. 13. Reaction of the 1989 spine-1 gas with fresh 1986 andesitic lava at 375°C. The abscissa shows the log gas/rock ratios. (a) Quantities of major alteration minerals formed (for mineral abbreviations see Fig. 11). (b, c) Log mole concentrations of dominant gaseous species.

silicates in the spine-1 alteration assemblages include tridymite, Al silicate, Fe-Al silicate, Ca-Mg silicate, Ca-Al silicate, Ca-Mg-Fe silicate, Ca silicate and a few multiple-cation silicates with S or Cl. Chemically similar phases produced by the 640°C gas–rock titrations include tridymite, Al silicate (andalusite),

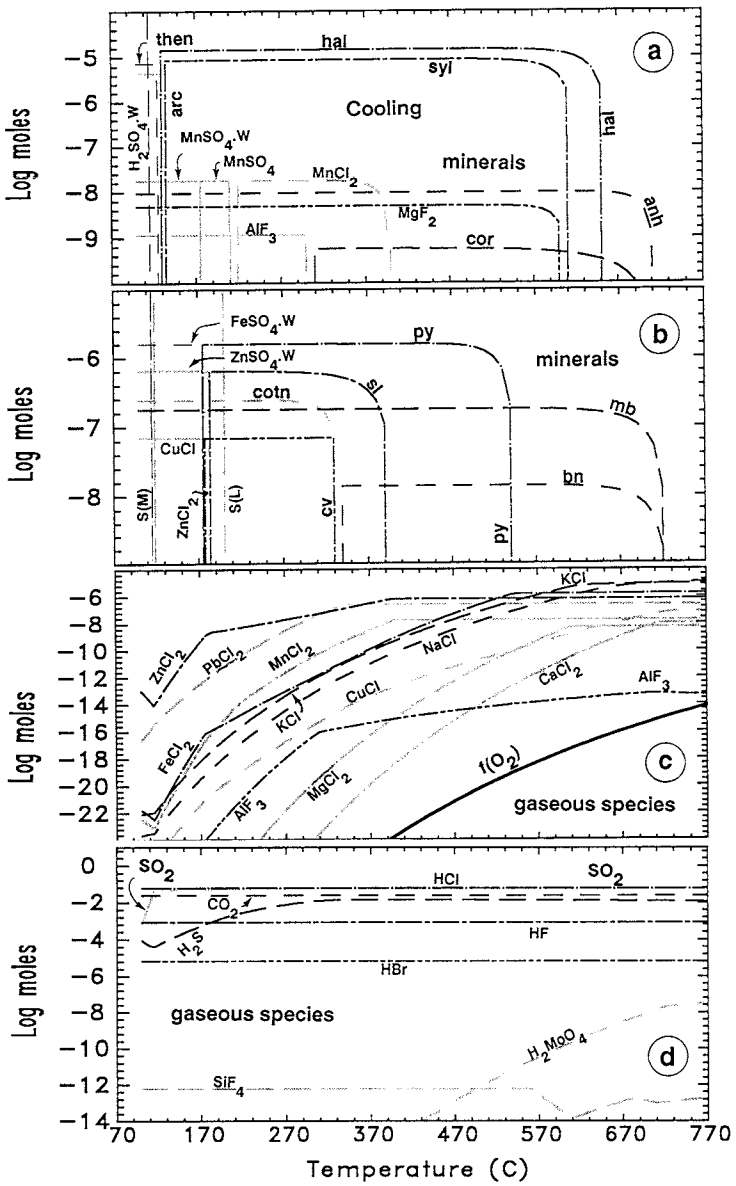

Fig. 14. Graph showing numerical cooling of Augustine 1987 dome-3 gas from 870 to 100°C without mineral fractionation. (a, b) Quantities of major sublimate minerals formed (for mineral abbreviations see Fig. 11). (c, d) Log mole concentrations of dominant gaseous species. The small gaps between curves where one mineral is replaced by another (e.g., between *AlF$_3$* and *cor*) is an artifact of the finite temperature step sizes used in the calculations.

Ca-Mg silicate (diopside), Ca-Al silicate (anorthite), Ca-Fe silicate (hedenbergite) and Ca silicate (wollastonite). Since we cannot tell the specific phase identities in the natural altered rocks, we cannot know whether the observed and computed assemblages match in detail. Further, the calculations do not take into account kinetic effects and our mineral data base, although large, is inevitably incomplete, making it possible to fail to match phases owing to a lack of the necessary thermodynamic data. Nevertheless, the compositional correspondence between the computed and observed silicates generally supports the idea that direct reactions of the primary gas with the rock plays a major role in forming the natural silicate assemblage.

Comparison of the natural to the computed systems is also hindered because the calculations examine a series of gas–rock batches at changing ratio of gas to rock, whereas the rock in the natural setting is exposed to a moving stream of gas. The gas/rock ratio provides only an approximate basis for comparison and it is hard to know what gas/rock ratio is most appropriate, but it is likely that a high g/r applies at the innermost edge of the fumarole, where tridymite is the dominant phase in the high-temperature fumaroles, accompanied by an aluminum silicate and unidentified phases containing Fe, Ca, Mg, K and Na (Table 1).

The 375°C gas–rock titration accounts for abundant silica minerals in the spine-3 alteration assemblages, although the calculation produces quartz instead of cristobalite and amorphous silica; in the natural setting, these minerals probably formed in lieu of quartz for kinetic reasons. Overall, we conclude that the volcanic gas–rock reaction might be the primary origin of the silicates in the spine-1 and spine-3 vents. The 640 and 375°C gas–rock titrations (Figs. 11–13) fail to account for the sulfates, oxides and halides observed in the spine-1 and spine-3 vents (Table 1), except perhaps anhydrite and halite which are calculated to form from rock-derived Ca and Na by addition of gas derived from sulfate (SO_2 disproportionation) and chloride (HCl). It is likely that much of the halite precipitated directly from the cooling gases because abundant halite is observed in silica-tube sublimates collected from the spine-1 vent (Symonds, unpubl.; Bernard, unpubl.). In contrast to the silicates, many of the sulfates, oxides and halides in the fumarole wall rocks are likely to form by cooling of metal-bearing volcanic gases or mixing of volcanic gases with air. These processes are explored below.

13. Heterogeneous equilibrium cooling of the 1987 dome-3 gas from 870 to 100°C

To test whether simple cooling of the volcanic gases could account for some minerals in these alteration assemblages, we executed a series of cooling-with-mineral-precipitation calculations. For the first set of calculations, we cool the 1987 gas composition (Table 9) to 100°C from the equilibrium temperature of 870°C. The calculations were executed both without and with mineral fractionation.

13.1. Cooling without mineral fractionation

Cooling of volcanic gases without mineral fractionation allows precipitated minerals to interact continuously with the gas. This simulates the formation of aerosols in the gas stream because the precipitates can continuously back-react with the cooling gases. During this calculation, minerals precipitate and dissolve as temperature decreases. This simulation yields precipitation of sulfides, chlorides, fluorides, sulfates, liquid and monoclinic sulfur and hydrated H_2SO_4 (Fig. 14).

13.1.1. Sulfides

With the exception of molybdenite, the sulfides precipitate between 700 and 175°C. Bornite (Cu_5FeS_4) and molybdenite (MoS_2) are among the first high-temperature minerals that start to precipitate around 700°C (Fig. 14b). They precipitate via the reactions:

$$5\,CuCl + FeCl_2 + 4\,SO_2 + \tfrac{23}{2}H_2 \Rightarrow$$

$$Cu_5FeS_4 + 7\,HCl + 8\,H_2O \quad (1)$$
(bn)

$$H_2MoO_4 + 2\,SO_2 + 7\,H_2 \Rightarrow MoS_2 + 8\,H_2O \quad (2)$$
(mb)

[The ⇒ symbol in reactions (1) and (2) and in the following reactions indicates a process driven by change in pressure, temperature, or composition.] The precipitation of these sulfides causes gaseous CuCl and H_2MoO_4 to decrease with falling temperature (Fig. 14c and d). Molybdenite precipitates until the calculation ends at 100°C, whereas bornite is replaced by covellite (CuS) at 330°C (Fig. 14b) following the reaction:

$$\underset{\text{(bn)}}{Cu_5FeS_4} + 3\,SO_2 + 6\,H_2 \Rightarrow 5\,\underset{\text{(cv)}}{CuS} + \underset{\text{(py)}}{FeS_2} + 6\,H_2O \quad (3)$$

Covellite precipitates until the gas cools to 175°C at which point it is replaced by CuCl(s) (Fig. 14b) by the reaction:

$$2\,\underset{\text{(cv)}}{CuS} + 2\,HCl \Rightarrow 2\,CuCl(s) + 2\,S(L) + H_2 \quad (4)$$

Pyrite starts precipitating around 540°C following the reaction:

$$FeCl_2 + 2\,SO_2 + 5\,H_2 \Rightarrow \underset{\text{(py)}}{FeS_2} + 2\,HCl + 4\,H_2O \quad (5)$$

It precipitates until 175°C when hydrated iron sulfate [$Fe_2(SO_4)_3 \cdot H_2O$(s)] replaces pyrite (Fig. 14b) following the reaction:

$$2\,\underset{\text{(py)}}{FeS_2} + 7\,SO_2 + 2\,H_2 \Rightarrow Fe_2(SO_4)_3 \cdot H_2O(s) + 8\,S(L) + H_2O \quad (6)$$

Sphalerite (ZnS) begins forming at 390°C following the reaction:

$$ZnCl_2 + SO_2 + 3\,H_2 \Rightarrow \underset{\text{(sl)}}{ZnS} + 2\,HCl + 2\,H_2O \quad (7)$$

and continues precipitating until it is replaced by zinc chloride [$ZnCl_2$(s)] at 180°C. The precipitation of sphalerite at ≤ 390°C causes the concentration of $ZnCl_2$ to decrease (Fig. 14c); $ZnCl_2$ decreases at an even sharper rate below 180°C when $ZnCl_2$(s) and $ZnSO_4 \cdot H_2O$(s) precipitate.

13.1.2. Chlorides

Halite (NaCl) and sylvite (KCl) are the dominant chlorides. Halite starts forming at 650°C and is the dominant precipitate until liquid sulfur forms at ≤ 200°C. It continues to precipitate until 120°C at which point it is replaced by thenardite (Na_2SO_4, Fig. 14a) via the reaction:

$$\underset{\text{(hal)}}{2\,NaCl} + 2\,SO_2 + H_2 \Rightarrow \underset{\text{(then)}}{Na_2SO_4} + 2\,HCl + S(L) \quad (8)$$

Sylvite starts precipitating at 610°C and is the second most abundant phase from 610 to 200°C. It forms until 130°C where it is replaced by arcanite (K_2SO_4, Fig. 14a) by the reaction:

$$\underset{\text{(syl)}}{2\,KCl} + 2\,SO_2 + H_2 \Rightarrow \underset{\text{(arc)}}{K_2SO_4} + 2\,HCl + S(L) \quad (9)$$

Unlike halite and sylvite, the other chlorides do not form until the temperature drops below 400°C (Fig. 14a and b). At 400°C, manganese chloride [$MnCl_2$(s)] appears; it precipitates until it is replaced by manganese sulfate [$MnSO_4$(s)] at 210°C (Fig. 14b).

Cotunnite ($PbCl_2$) precipitates at 330°C if $PbCl_4$ and $PbBr_4$ are suppressed (Fig. 14b). We suppress $PbCl_4$ and $PbBr_4$ because the enthalpies of formation for these species have large uncertainties, and including them in the cooling calculations terminates precipitation of all Pb-bearing solids (Symonds and Reed, 1993).

Zinc chloride [$ZnCl_2$(s)] starts forming at 180°C, replacing sphalerite (Fig. 14b). At 175°C it is replaced by hydrated zinc sulfate [$ZnSO_4 \cdot H_2O$(s), Fig. 14a].

CuCl(s) is the last chloride to precipitate (Fig. 14b). It replaces covellite at 175°C by reaction (4). By approximately 110°C, most of the metal chlorides were replaced by sulfates or their hydrates and the gaseous chloride species increase sharply (Fig. 14c).

13.1.3. Fluorides

Two fluorides, $MgF_2(s)$ and $AlF_3(s)$, precipitate in this cooling calculation. $MgF_2(s)$ starts to precipitate at 600°C (Fig. 14a). Its precipitation, from 600 to 100°C, extracts significant $MgCl_2$ from the gas (Fig. 14c) following the reaction:

$$MgCl_2 + 2\,HF \Rightarrow MgF_2(s) + 2\,HCl \quad (10)$$

$AlF_3(s)$ starts forming at 300°C where it replaces corundum (Fig. 14a) by the reaction:

$$Al_2O_3\ (cor) + 6\,HF \Rightarrow 2\,AlF_3(s) + 3\,H_2O \quad (11)$$

13.1.4. Sulfates

Except anhydrite ($CaSO_4$) which forms at 710°C, all sulfates form below 210°C (Fig. 14a). Anhydrite's early appearance depletes Ca from the gas (Fig. 14c) following the reaction:

$$CaCl_2 + SO_2 + 2\,H_2O \Rightarrow CaSO_4\ (anh) + 2\,HCl + H_2 \quad (12)$$

$MnSO_4(s)$ replaces $MnCl_2(s)$ at 210°C by the reaction:

$$MnCl_2(s) + SO_2 + 2\,H_2O \Rightarrow MnSO_4(s) + 2\,HCl + H_2 \quad (13)$$

At 175°C, $MnSO_4(s)$ is replaced by the hydrate, $MNSO_4 \cdot H_2O(s)$ (Fig. 14b). At the same temperature (175°C) hydrous sulfates of iron and zinc also precipitate, replacing pyrite by reaction (6) and zinc chloride by the reaction:

$$ZnCl_2(s) + 3\,SO_2 + 3\,H_2 \Rightarrow ZnSO_4 \cdot H_2O(s) + 2\,HCl + 2\,S(L) + H_2O \quad (14)$$

Arcanite and thenardite, two common phases in fumarolic incrustations, also precipitate in this cooling calculation. Arcanite starts forming at 130°C, replacing sylvite by reaction (9) and thenardite replaces halite at 120°C, by reaction (8) (Fig. 14a). Both alkali sulfates precipitate until the calculation ends at 100°C.

13.1.5. Sulfur

Liquid sulfur forms at 210°C. It dominates the precipitates until it is replaced by monoclinic sulfur at 119°C (Fig. 14b). Like the liquid sulfur, crystalline native sulfur also dominates the precipitates until hydrated sulfuric acid forms at 114°C. These phases form by the following reactions:

$$SO_2 + 2\,H_2S \Rightarrow 3\,S(L) + 2\,H_2O \quad (15)$$

$$S(L) \Rightarrow S(M) \quad (16)$$

13.1.6. Hydrated sulfuric acid

The deposition of $H_2SO_4 \cdot 6\,H_2O(l)$ at 114°C heralds the extremely acidic conditions of the system below 114°C (Fig. 14a). It forms by the reaction:

$$SO_2 + 8\,H_2O \Rightarrow H_2SO_4 \cdot 6\,H_2O(l) + H_2 \quad (17)$$

$H_2SO_4 \cdot 6\,H_2O(l)$ and monoclinic sulfur are the dominant phases in the system at ≤ 114°C. In volcanic fumaroles, these sulfuric acid aerosols coat the wall rock and trigger severe acid leaching and alteration of the fumarole wall rocks (e.g., Stoiber and Rose, 1974).

13.2. Cooling with mineral fractionation

Cooling of volcanic gases with mineral fractionation disallows the interaction of mineral precipitates with the remaining gas. Precipitated minerals are removed after each temperature step. This capability of GASWORKS is used to model the precipitation and removal of sublimates along fumarolic pathways (Symonds and Reed, 1993).

13.2.1. Sulfides

Molybdenite and bornite which start precipitating at 725°C, are the highest-temperature sublimates. After their initial peak deposition, the precipitation rates of these sulfides decrease sharply owing to mineral fractionation (Fig. 15b). The deposition of molybdenite and bornite causes immediate depletion of copper and molybdenum from the gas in response to reactions (1) and (2) (Fig. 15c and d). At 330°C, bornite is superseded by the precipitation of covellite

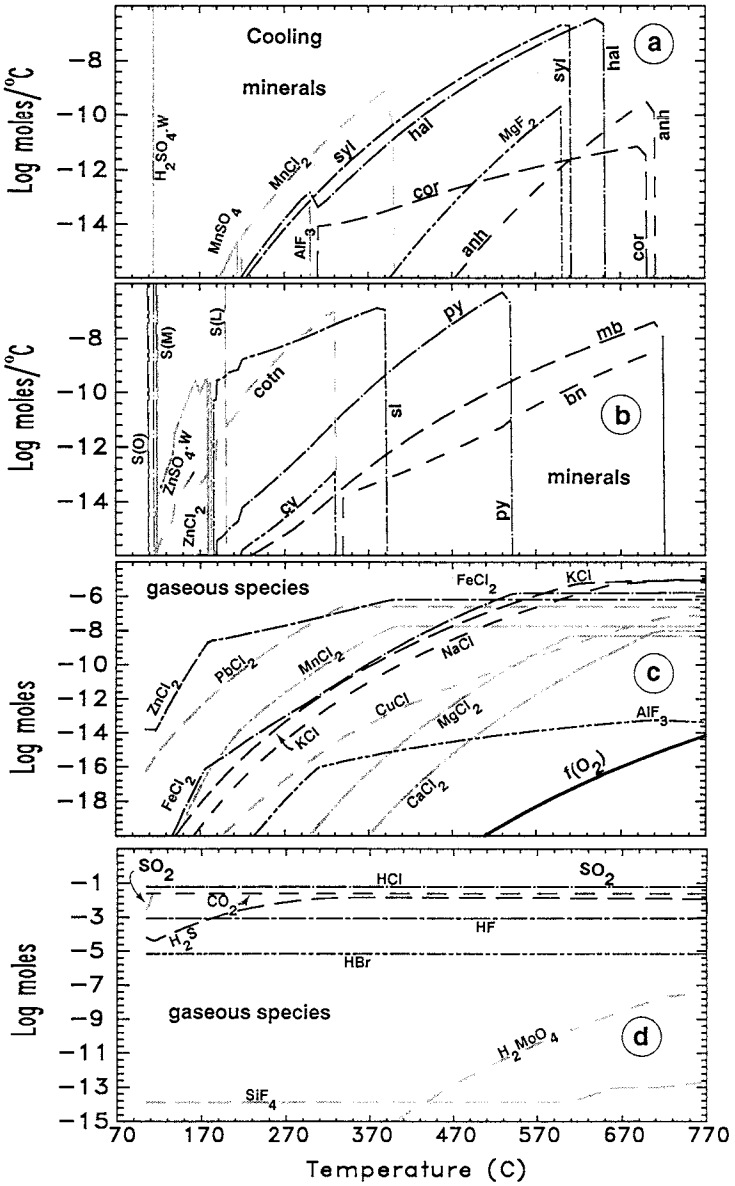

Fig. 15. Graph showing numerical cooling of the 1987 dome-3 gas from 870 to 100°C with mineral fractionation. (a, b) Quantities of major minerals formed (for mineral abbreviations see Fig. 11). (c, d) Log mole concentrations of dominant gaseous species.

which precipitates directly from the dominant Cu-bearing gas species by the following reaction:

$$\tfrac{1}{3}(CuCl)_3 + SO_2 + \tfrac{5}{2}H_2 \Rightarrow \underset{(cv)}{CuS} + HCl + 2H_2O \quad (18)$$

With further cooling, covellite decreases in abundance until CuCl(s) precipitates at 180°C (Fig. 15b) by the reaction:

$$\tfrac{1}{3}(CuCl)_3 \Rightarrow CuCl(s) \quad (19)$$

Such reactions [e.g., (18) and (19)] depict the precipitation of minerals during the cooling-with-fractionation calculations. Notice that, in contrast to the cooling-without-fractionation calculations, they are not true replacement reactions because the phase that would be replaced is separated from the system. These solids precipitate directly from the appropriate metal-bearing gas species.

Large amounts of pyrite start precipitating at 540°C, and at 175°C hydrated iron sulfate starts to precipitate following reaction:

$$2FeCl_3 + 7SO_2 + 5H_2 \Rightarrow Fe_2(SO_4)_3 \cdot H_2O(s) + 6HCl + 4S(L) + H_2O \quad (20)$$

Fractionation of pyrite strips the gas of Fe (Fig. 15c), and by 175°C, where hydrated iron sulfate forms, iron is largely removed from the gas (Fig. 15c).

Sphalerite (ZnS) dominates the sulfides after it starts precipitating at 390°C, specifically following reaction (7); it continues to precipitate until 180°C where $ZnCl_2(s)$ (Fig. 15b) precipitates. In this calculation, most of the sulfides with the exception of sphalerite, precipitate in abundance only at higher temperatures; their abundances decrease with cooling as they are fractionated from the system (Fig. 15a and b).

13.2.2. Chlorides

Halite and sylvite are the first chlorides to form (Fig. 15a), halite at 650°C, followed by sylvite at 640°C. Halite is the dominant chloride until sylvite precipitates. The precipitation of these alkali chlorides depletes K and Na from the gas as shown in Fig. 15c. At lower temperature (130–120°C), potassium and sodium sulfates form:

$$2KCl + 2SO_2 + H_2 \Rightarrow \underset{(arc)}{K_2SO_4} + 2HCl + S(L) \quad (21)$$

$$2NaAlF_4 + 3SO_2 + 3H_2 \Rightarrow \underset{(then)}{Na_2SO_4} + 2AlFO + 6HF + 2S(L) \quad (22)$$

$MnCl_20(s)$ is the dominant chloride from 400 to 210°C (Fig. 15a). At 210°C, manganese sulfate precipitates following reaction:

$$MnCl_2 + SO_2 + 2H_2O \Rightarrow MnSO_4(s) + 2HCl + H_2 \quad (23)$$

The fractionation of these minerals strips the gas of manganese (Fig. 15c). At 180°C, $ZnCl_2(s)$ becomes the dominant chloride, but it is supplanted by the precipitation of hydrated zinc sulfate (Fig. 15a). CuCl(s) also forms at 180°C, directly from $(CuCl)_3$ gas following reaction (19).

13.2.3. Fluorides

Among fluorides, gas cooling yields $MgF_2(s)$ at 600°C [reaction (10), Fig. 15a] and $AlF_3(s)$, which starts to precipitate at 300°C (Fig. 15a) following reaction:

$$AlFO + 2HF \Rightarrow AlF_3(s) + H_2O \quad (24)$$

13.2.4. Sulfates

Anhydrite starts precipitating at 712°C by reaction (12) and is the earliest sulfate to form. Its abundance decreases rapidly with cooling (Fig. 15a), but it continues to precipitate until gypsum (not shown in Fig. 15b) precipitates at 125°C. Other sulfates precipitate below 210°C including $MnSO_4(s)$ at 210°C, $MnSO_4 \cdot H_2O(s)$ and hydrous sulfates of iron and zinc at 180°C (Fig. 15b).

Arcanite and thenardite precipitate at 140°C [reactions (21) and (22)] in very small amounts because of the previous extraction of potassium and sodium

from the gas by precipitation of sylvite and halite (Fig. 15a).

13.2.5. Sulfur and sulfuric acid

Liquid sulfur appears at 205°C, becoming the dominant phase (Fig. 15b). Monoclinic sulfur starts to precipitate at 119°C (Fig. 15b) and is supplanted at 115°C by orthorhombic sulfur. $H_2SO_4 \cdot 6H_2O(l)$ also forms at 115°C with orthorhombic sulfur; together they dominate the system (Fig. 15b). The deposition of $H_2SO_4 \cdot 6H_2O(l)$ depletes the system of sulfate precluding the precipitation of all other sulfates.

14. Heterogeneous equilibrium cooling of the 1989 gas from 757 to 100°C

We repeated the above cooling calculations using the 1989 gases, since some phases in the altered spine-1 and spine-3 rocks may have been deposited relatively recently. This also allows us to test the sensitivity of the cooling calculations by using a somewhat different gas composition. For these calculations, we cool the average 1989 gas composition (Table 9) from the equilibrium temperature of 757 to 100°C both without and with mineral fractionation. The results of both calculations are shown in Fig. 16.

As the gas cools from the equilibrium temperature (757°C), diopside, bornite and heazlewoodite (Ni_3S_2) precipitate. With further cooling to 690°C, heazlewoodite is replaced by millerite (NiS). Between 670 and 590°C, molybdenite, halite and sylvite start forming. Halite and sylvite are the dominant minerals between 670 and 140°C in the cooling-without-fractionation case (Fig. 16a and b) and between 630 and 450°C in the cooling-with-fractionation calculation (Fig. 16c and d). Anhydrite starts forming at 590 and 490°C in the fractionation and non-fractionation cases, respectively. It is the only sulfate mineral that forms at high temperature (Fig. 16). The high-temperature assemblage consists dominantly of sulfides of Cu, Ni, Mo, Zn, Pb, Cd, Fe and Mn. Some of these sulfides (PbS, CdS and MnS) are replaced by chlorides below 310°C (Fig. 16). At 195°C, $MnCl_2(s)$ is replaced by $MnSO_4(s)$ which is replaced by $MnSO_4 \cdot H_2O(s)$ at 170°C (Fig. 16). Orpiment (As_2S_3) forms at 250°C and becomes the dominant mineral species in the fractionation calculation between 250 and 150°C (Fig. 16d).

Liquid and crystalline sulfur are the abundant low-temperature precipitates (Fig. 16a and c), but in contrast to the 1987 dome-3 gas cooling calculation, $H_2SO_4 \cdot 6H_2O(l)$ does not form in this calculation.

15. Mixing of Augustine gas with air

Thermochemical modeling of volcanic gases mixing with air enable us to study the effects of air in forming incrustations. Volcanic gases may mix with air that became entrained within the fumarole through fractures around the base of the dome or with air surrounding the fumarole orifices. In the case of the spine-1 and spine-3 vents, most of the air addition apparently occurs at the fumarolic orifices because the gases contain only small amounts of air (Symonds et al., 1990).

For this calculation, we begin with the compositions of the volcanic gas and air, and their respective initial temperatures. Each mixing step is computed by adding an increment of air to the volcanic gas. Program GASWORKS then determines the temperature of the bulk gas and calculates the distribution of mineral and gas species.

15.1. Mixing of Augustine's 1987 dome-3 gas with air

The mixing of the 870°C dome-3 gas with 25°C air produces abundant sulfates, oxides, hydrated sulfates, hydrated sulfuric acid and minor fluorides. At the relatively large log gas/air (log/a) ratio of 0.72 (729°C), thenardite, arcanite, hematite and anhydrite form (Fig. 17a). Thenardite is the dominant precipitate until $H_2SO_4(l)$ precipitates at a log g/a ratio of −0.6. The precipitation of alkali sulfates strips NaCl and KCl from the gas (Fig. 17b). $CaCl_2$ also decreases sharply owing to the precipitation of anhydrite (Fig. 17b). At a log g/a ratio of 0.4 (628°C) hematite is replaced by $Fe_2(SO_4)_3(s)$, and $MnSO_4(s)$,

chalcocyanite ($CuSO_4$) and MgF_2(s) also start to precipitate. The precipitation of these oxides, sulfates and fluorides causes a severe depletion of Fe, Mn, Cu and Mg from the gas (Fig. 17b). As more air is added, cotunnite ($PbCl_2$) and zinkosite ($ZnSO_4$) precipitate at 588 and 522°C, respectively (Fig. 17a), depleting the gas of $PbCl_2$ and $ZnCl_2$ (Fig. 17c). Zinkosite and chalcocyanite are replaced by $ZnSO_4$ ·

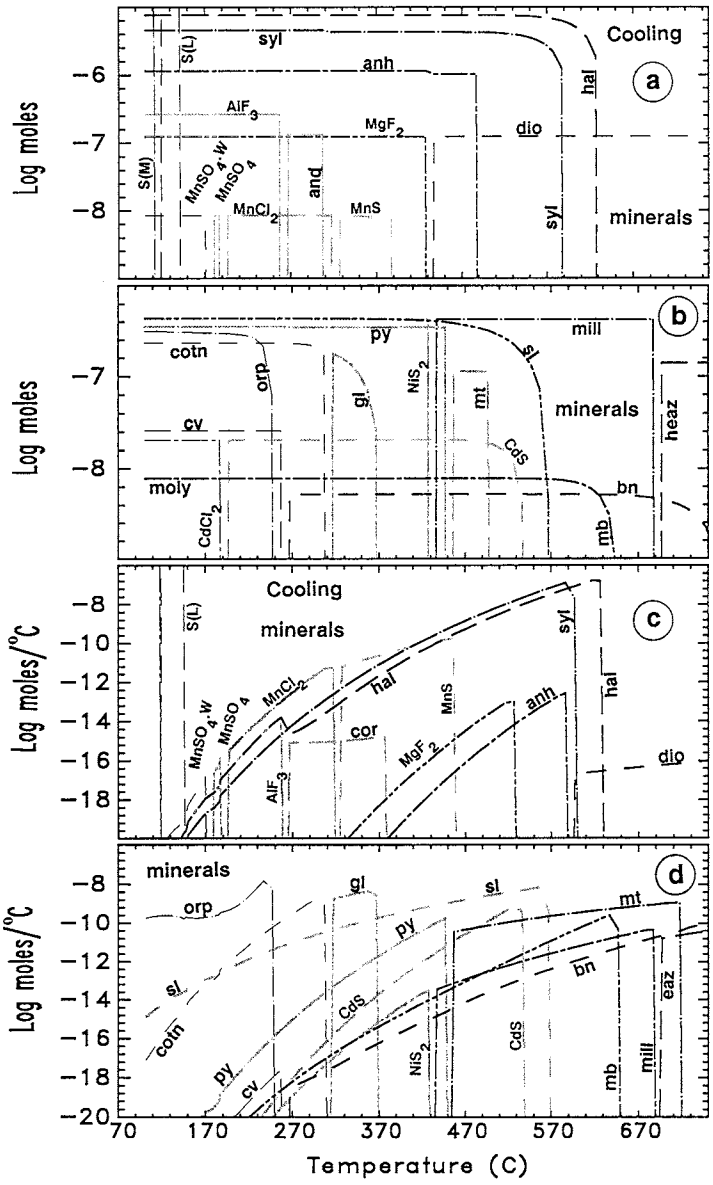

Fig. 16. Graph showing numerical cooling of the 1989 spine-1 gas from 757 to 100°C without and with mineral fractionation. (a, b) Quantities of major sublimate minerals formed during cooling without mineral fractionation. (c, d) Quantities major minerals formed during cooling with mineral fractionation (for mineral abbreviations see Fig. 11).

H_2O(s) and $CuSO_4 \cdot H_2O$(s) at 209 and 158°C, respectively (Fig. 17a). Another near-200°C precipitate includes $H_2SO_4 \cdot H_2O$(l), which forms at 210°C (Fig. 17a). Molybdite (MoO_3) starts precipitating at 181°C and is the only oxide that forms below 628°C.

The log f_{O_2} increases steeply from its starting value of −12.60 in the 870°C volcanic gas to −2.00 at a log g/a ratio of 0.7. Then, f_{O_2} increases gradually to −0.78 as the log g/a ratio decreases to −0.85 and the temperature drops to 129°C (Fig. 17c).

15.2. Mixing of Augustine's 1989 gas with air

Mixing of the 757°C 1989 gas with 25°C air produces abundant sulfates and oxides (Fig. 18). Magnetite forms at relatively large gas/air ratios (> 722°C), but is replaced by hematite at 722°C (Fig. 18). Hematite continues precipitating until it is replaced by $FeSO_4$(s) at 530°C (log g/a = 0.4). Thenardite and arcanite are by far the dominant minerals formed in the cooling-without-fractionation calculation (Fig. 18a). In the cooling-with-fractiona-

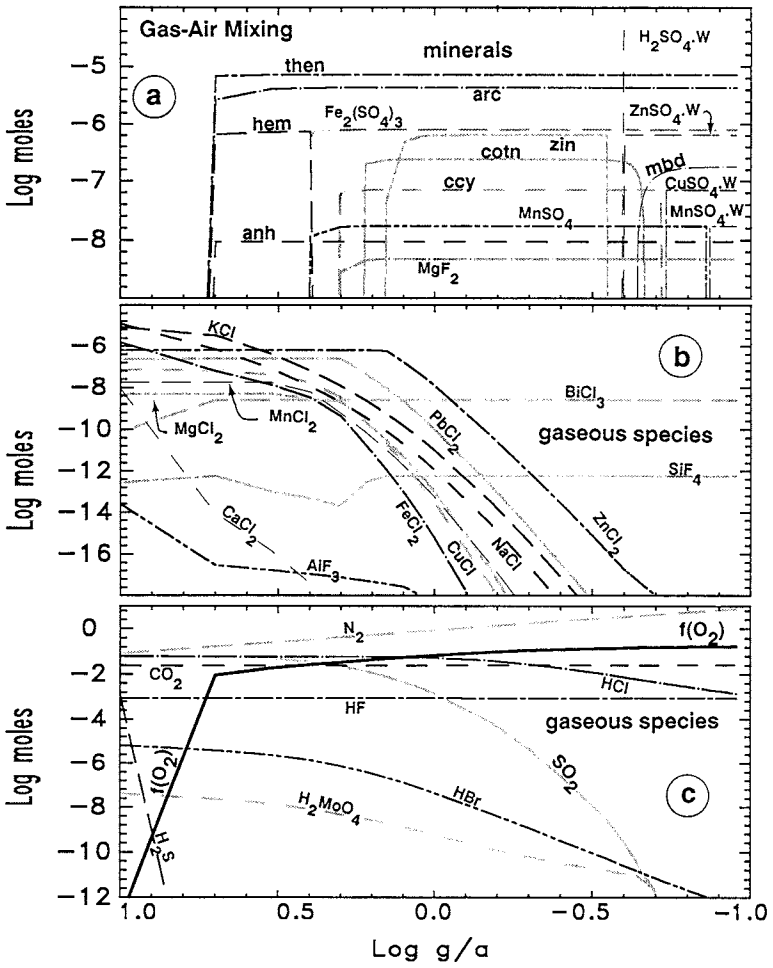

Fig. 17. Diagram showing numerical mixing of the 870°C 1987 dome-3 gas with 25°C air. The abscissa shows the log gas/air ratios. (a) Quantities of major minerals formed during the air-mixing calculation (for mineral abbreviations see Fig. 11). (b, c) Log mole concentrations of dominant gaseous species.

tion case there is a predominance of thenardite and arcanite from 722 to 635°C (log g/a ratios of 1.32 to 0.7), anglesite ($PbSO_4$) from 635 to 567°C (log g/a ratios of 0.7 to 0.46), zinkosite and As_2O_5(s) from 567 to 288°C (log g/a ratios of 0.46 to 0.05), and Sb_2O_4(s) below 288°C (Fig. 18b). Most of the oxides that form at high gas/air ratios are replaced by their respective sulfates at low gas/air ratios.

16. Comparisons of calculated results with observed sublimates

One way to check the validity of the cooling calculations is to compare them with the sublimates collected from Augustine volcano in 1987 and 1989. Such comparisons help discriminate which incrustation phases form by simple cooling of volcanic gases and which solids form by more complex processes. To isolate and characterize the minerals that precipitate directly from cooling volcanic gases, sublimates can be collected using the silica-tube method (Le Guern and Bernard, 1982). Silica-tube sublimates were collected from high-temperature dome fumaroles in 1987 from the 870°C spine-1 vent (Symonds, unpubl.) and in 1989 from spine-1 (640°C), spine-2 (563°C) and spine-3 (375°C; Bernard, unpubl.). The 1987 silica-tube sublimates display four zones (870–400°C): (1) cristobalite and magnetite; (2) halite, sylvite, molybdenite, bornite, cristobalite, magnetite and acmite; (3) halite, sylvite, pyrite, cristobalite and bornite; and (4) halite, sylvite, cristobalite, a Fe-K-Cu-S phase and CuCl(s) (Symonds, unpubl.). The 1989 sublimates collected inside silica tubes on the andesitic lava dome at Augustine exhibit major amounts of Na, K, Cu, Zn and Pb chlorides along with minor sulfides of Mo, Fe and Ni (Bernard, unpubl.).

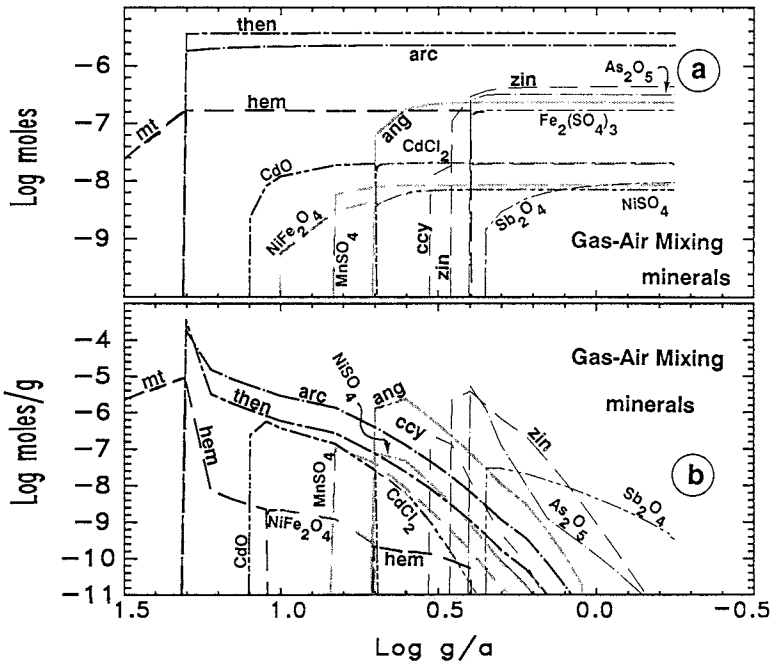

Fig. 18. Diagram showing numerical mixing of the 757°C 1989 spine-1 gas with 25°C air. The abscissa shows the log gas/air ratios. (a) Quantities of major minerals formed during the air-mixing without mineral fractionation calculation. (b) Log moles of dominant minerals formed during air-mixing with mineral fractionation calculation (for mineral abbreviations see Fig. 11).

The 1987 cooling calculations generally match the identity and zoning in the 1987 silica-tube sublimates. However, the modeling does not account for magnetite, cristobalite and Fe-K sulfide; as discussed by Symonds and Reed (1993), these discrepancies may reflect errors in the input gas composition (e.g., for Fe), or missing gases (e.g., H_4SiO_4) or solids (e.g., Fe-K sulfides) in the thermochemical data base, GASTHERM. The 1989 cooling calculations are also successful in predicting the observed 1989 sublimates and account for the greater abundances of Cu, Zn and Pb chlorides and Ni sulfides in the 1989 silica-tube deposits. Both the 1987 and 1989 cooling calculations predict the abundant native sulfur that is observed in the dome fumarole field.

To understand the phases that form when volcanic gases mix with air, Bernard (unpubl.) also studied the solids that precipitated on the external wall of the 1989 silica tubes. His external-wall solids grade from a hot-reduced assemblage of mixed oxides and chlorides to a cooler-oxidized assemblage of Na and K sulfates mixed with cassiterite (SnO_2) and anglesite. Our volcanic gas–air mixing calculations indicate a predominance of Na and K sulfates and a subordinate amounts of Zn, Pb, Fe and Cu sulfates along with oxides of Fe, Cd, As and Sb (Fig. 17). As temperature decreases and oxidation increases, most of these sulfates are replaced by hydrated forms, as exhibited by the 1987 gas–air mixing calculations (Fig. 17). The absence of cassiterite is expected since we did not incorporate Sn in our starting gas composition.

Hydrated sulfuric acid is dominant over the low-temperature range in both the simple cooling and the volcanic gas–air mixing calculations of the 1987 gases. Its stability increases significantly with decreasing temperature and with increasing air dilution (Fig. 14, Figs. 15 and 17).

In general, excellent agreement exists between the simple cooling calculations and the sublimates observed within the silica tubes. Excellent agreement also exists between the 1989 volcanic gas–air mixing calculations (Fig. 18) and the phases observed on the outer walls of the 1989 silica tubes. This overall correspondence is evidence that the equilibrium calculations predict the identity and zoning of the various phases precipitated on the inner and outer walls of the silica tubes. This suggests that most chlorides, sulfates and low-valence oxides form by simple cooling of volcanic gases. In contrast, many sulfates and their hydrates as well as high-valence oxides form when volcanic gases mix with air.

17. Summary and conclusions

The color banding exhibited by the pneumatolytically altered wall rocks in Augustine's fumaroles reflect their complex environments of formation. These color zones mark mineral assemblages that form by various chemical and physical processes within and around volcanic fumaroles. XRD, EDS and microprobe analyses of these incrustation assemblages reveal abundant crystalline minerals and minor amounts of amorphous solids, including oxides, hydroxides, chlorides, sulfates and silicates of Ca, Mg, Fe, K, Na, Al and Ti.

Distinct mineral zones form by direct reaction of volcanic gases with the wall rock, cooling of volcanic gases, mixing of volcanic gases with air and/or a combination of these processes (e.g., Stoiber and Rose, 1974; Thomas et al., 1982; Varekamp et al., 1986; Rose, 1987; Quisefit et al., 1988; Getahun et al., 1992; Symonds and Reed, 1993). These processes were explored in model calculations of gas–rock reactions, cooling of the volcanic gases and mixing of air with the volcanic gases.

A comparison of model results to the observed alteration assemblages suggests the following:

(a) Direct volcanic gas–rock reaction at 640°C produces abundant tridymite and some silicates at high g/r ratios. The high-temperature (spine-1) alteration assemblages at Augustine are dominantly composed of tridymite, Al silicate (Al-Si phase) and various unidentified silicates. The silicates that precipitate in the gas–rock reaction resemble the compositions of the identified high-temperature silicates in the spine-1 alteration zones.

(b) Cooling produces dominantly halite and sylvite over a large temperature range, suggesting that the halite and sylvite in the alteration assemblages precipitated directly from the cooling volcanic gases. This is consistent with their euhedral crystal forms (e.g., Fig. 5b) that match the morphologies of halite and sylvite in silica-tube sublimates (Symonds,

1993). Simple cooling calculations predicted the sulfides and chlorides observed in the silica-tube sublimates, so it seems likely that these phases in the natural incrustations form by simple cooling of volcanic gases.

(c) The volcanic gas–air mixing calculations generally produce Na, K and Ca sulfates and iron oxide at high g/a ratios. As the g/a ratio decreases sulfates of Pb, Zn, Cu and Fe form. Addition of even more air, with consequent cooling produces hydrated sulfates.

(d) The modeling shows that all of the hydrated sulfates and some of the anhydrous sulfates form at low temperatures and low g/a ratios. These phases are observed in the low-temperature zone in the spine-3 vent, implying that most of the hydrated sulfates and a few anhydrous sulfates form by the volcanic gas–air reaction at low g/a ratios.

(e) At low temperature, between 115 and 200°C, hydrated sulfuric acid is predicted to be a dominant phase, which is consistent with previous studies (e.g., Stoiber and Rose, 1974; Symonds et al., 1992). The formation of sulfuric acid in low-temperature fumaroles initiates acidic wall rock alteration in these vents.

Even though these calculations do not entirely duplicate the fumarolic alteration processes, they put significant constraints on the various processes that might have formed the zoned alteration sequences in the wall rock of Augustine's fumaroles. In particular, the modeling has successfully demonstrated that the mineral content and zoning of the fumarole wall rock may have been caused by the interplay of a continuous gas–rock reaction, cooling of volcanic gases and mixing of volcanic gases with air.

Acknowledgements

The first author is grateful to Fulbright Scholarship Commission for financial support during this study and in particular to Mrs. Paula Carter, Institute of International Education Regional Office Representative. Support for this research was also provided by NSF grant to Mark Reed, EAR-8915854. We thank T.E.C. Keith, J.M. Thompson, E.W. Wolfe and the JVGR reviewers for thier most helpful reviews of the manuscript.

References

Beget, J.E. and Kienle, J., 1992. Cyclic formation of debris avalanches at Mount St. Augustine volcano. Nature, 356: 701–704.

Buffler, R., 1975. Geology of the south side of Augustine Island, Alaska. State Alaska Div. Geol. Geophys. Rep. Invest.

Casadevall, T.J., Rose, W.I., Gerlach, T., Greenland, L.P., Ewert, J., Wunderman, R. and Symonds, R.B., 1983. Gas emissions and the eruptions of Mount St. Helens through 1982. Science, 221: 1383–1385.

Cullers, R.L. and Graf, J.L., 1984. Rare earth elements in igneous rocks of the continental crust: Intermediate and silicic rocks — Ore petrogenesis. In: P. Henderson (Editor), Rare Earth Element Geochemistry. Elsevier, Amsterdam, pp. 275–316.

Detterman, R.L., 1973. Geologic map of the Iliamna B-2 Quadrangle, Augustine Island, Alaska. U.S. Geol. Surv. Map GQ-1068.

Gerlach, T.M., 1980a. Evaluation of volcanic gas analysis from Kilauea Volcano. J. Volcanol. Geotherm. Res., 7: 295–317.

Gerlach, T.M., 1980b. Investigation of volcanic gas analysis and magma out gassing from Erta'Ale lava lake, Afar, Ethiopia. J. Volcanol. Geotherm. Res., 7: 415–441.

Getahun, A., 1994. Fluid–rock reaction and mineralization in two high-level volcanic settings: Augustine fumaroles and the Summitville acid-sulfate copper-gold deposit. Ph.D. Diss., Univ. Oregon, 332 pp.

Getahun, A., Reed, M.H. and Symonds, R.B., 1992. Augustine volcano fumarole wall rock alteration: mineralogy, zoning and numerical models of its formation process. In: Y.K. Kharaka and A.S. Maest (Editors), Water–Rock Interaction. Proc. 7th Int. Symp. on Water–Rock Interaction, Balkema, Rotterdam, pp. 1411–1414.

Harris, D.M., Sato, M., Casadevall, T.J., Rose Jr., W.I. and Bornhorst, T.J., 1981. Emission rates of CO_2 from plume measurements. In: P.W. Lipman and D.R. Mullineaux (Editors), The 1980 Eruptions of Mount St. Helens, Washington. U.S. Geol. Surv. Prof. Pap., 1250: 17–30.

Holloway, J.R. and Burnham, C.W., 1972. Melting relations of basalt with equilibrium pressure less than total pressure. J. Petrol., 13: 1–29.

Humphris, S.E., 1984. The mobility of the rare earth elements in the crust. In: P. Henderson (Editor), Rare Earth Element Geochemistry. Dev. Geochem., 2: 317–342.

Johnston, D., 1978. Volatiles magma mixing and explosive mechanism of Augustine Volcano, Alaska. Ph.D. Thesis, Univ Washington, 177 pp.

Johnston, D., 1980. Volcanic contribution of chlorine to the Stratosphere: more significant to ozone than previously estimated? Science, 209: 491–492.

Keith, T.E.C., 1991. Fossil and active fumaroles in the 1912 eruptive deposits, Valley of Ten Thousands Smokes, Alaska. J. Volcanol. Geotherm. Res., 45: 227–254.

Kienle, J., 1986. Augustine Volcano. EOS Trans. AGU, 67: 804.

Kienle, J. and Swanson, S.E., 1985. Volcanic hazards from future eruptions of Augustine Volcano, Alaska. Geophys. Inst., Univ. Alaska, Fairbanks, AK, Rep. UAGR-275, 122 pp.

Kienle, J., Davies, J.N., Miller, T.P. and Yount, M.E., 1986. Eruption of Augustine Volcano: Public safety response by Alaskan volcanologists. EOS Trans. AGU, 67: 580–582.

Kodosky, L. and Keskinen, M., 1990. Fumarole distribution, morphology and incrustation mineralogy associated with the 1986 eruptive deposits of Mount St. Augustine Alaska. Bull. Volcanol., 52: 175–185.

Kodosky, L.G., Motyka, R.L. and Symonds, R.B., 1991. Fumarolic emissions from Mount St. Augustine, Alaska: 1979–1984 degassing trends, volatile sources and their possible role in eruptive style. Bull. Volcanol., 53: 381–394.

Krauskopf, K.B., 1964. The possible role of volatile metal mpounds in ore genesis. Econ. Geol., 59: 22–45.

Le Guern, F., 1988. Ecoulements gazeux reactifs a hautes temperatures measures et modelisation. Ph.D. Diss., Univ. Paris.

Le Guern, F. and Bernard, A., 1982. A new method for sampling and analyzing volcanic sublimates — application to Merapi volcano, Java. J. Volcanol. Geotherm. Res., 12: 133–146.

Lepel, E., Stefansson, K. and Zoller, W., 1978. The enrichment of volatile elements in the atmosphere by volcanic activity: Augustine Volcano 1976. J. Geophys. Res., 83: 6213–6220.

Marsh, B.D., 1982. The Aleutian. In: R.S. Thorpe (Editor), Andesites: Orogenic Andesites and Related Rocks. Wiley, New York, NY, pp. 99–114.

Quisefit, J.P., 1988. Physico-chimie de l'aerosol volcanique. Modelisation thermochimique du refroidissement des emanations de haute temperature. Ph.D. Diss., Univ. Paris, 258 pp.

Quisefit, J.P., Bergametti, G., Tedesco, D., Pinart, J. and Colin, L., 1988. Origin of particulate potassium in Mt. Etna emissions before and during the 1983 eruption. J. Volcanol. Geotherm. Res., 35: 111–119.

Quisefit, J.P., Toutain, J.P., Bergametti, G., Javoy, M., Cheynet, B. and Person, A., 1989. Evolution versus cooling of gaseous volcanic emissions from Momotombo Volcano, Nicaragua: Thermochemical model and observations. Geochim. Cosmochim. Acta, 53: 2591–2608.

Reed, M.H., 1982. Calculation of multicomponent chemical equilibria and reaction processes in systems involving minerals, gases and aqueous phase. Geochim. Cosmochim. Acta, 46: 513–528.

Reed, M.H., 1992. Origin of diverse hydrothermal fluids by reaction of magmatic volatiles with wall rock. Geol. Surv. Jpn. Rep., 279: 135–140.

Rose, W.I., 1987. Active pyroclastic processes studied with scanning electron microscopy. In: J.R. Marshall (Editor), Clastic Particles: Scanning Electron Microscopy and Shape Analysis of Sedimentary and Volcanic Clasts. Van Nostrand Reinhold, New York, NY, pp. 136–158.

Rose, W.I., Heiken, G., Wohletz, K., Eppler, D., Barr, S., Miller, T., Chuan, R.L. and Symonds, R.B., 1988. Direct rate measurements of plumes at Augustine volcano: A problem of scaling and uncontrolled variables. J. Geophys. Res., 93: 4485–4499.

Stoiber, R.E. and Rose, W.I., 1974. Fumarole incrustation at active Central American Volcanoes. Geochim. Cosmochim. Acta, 38: 495–516.

Sutton, A.J., McGee, K.A., Casadevall, T.J. and Stokes, J.B., 1992. Fundamental volcanic-gas-study techniques: An integrated approach to monitoring. In: J.E. Ewert and D.A. Swanson (Editors), Monitoring Volcanoes: Techniques and Strategies used by the Staff of the Cascades Volcano Observatory, 1980–1990. U.S. Geol. Surv. Bull., 1966: 181–188.

Swanson, S.E. and Kienle, J., 1988. The 1986 eruption of Mount St. Augustine: Field test of a hazard evaluation. J. Geophys. Res., 93: 4500–4520.

Symonds, R.B., 1993. Scanning electron microscope observations of sublimates from Merapi volcano, Indonesia. Geochem. J., 26: 341–354.

Symonds, R.B. and Reed, M.H., 1993. Calculation of multicomponent chemical equilibria in gas–solid–liquid systems: calculation methods, thermochemical data and applications to studies of high-temperature volcanic gases with examples from Mount St. Helens. Am. J. Sci., 293: 758–864.

Symonds, R.B., Rose, W.I., Reed, M.H., Lichte, F.E. and Finnegan, D.L., 1987. Volatilization, transport and sublimation of metallic and non-metallic elements in high temperature gases at Merapi Volcano, Indonesia. Geochim. Cosmochim. Acta, 51: 2083–2101.

Symonds, R.B., Rose, W.I. and Reed, M.H., 1988. Contribution of Cl- and F-bearing gases to the atmosphere by volcanoes. Nature, 334: 415–418.

Symonds, R.B., Rose, W.I., Gerlach, T.M., Briggs, P.H. and Harmon, R.S., 1990. Evaluation of gases, condensates and SO_2 emissions from Augustine Volcano, Alaska: the degassing of a Cl-rich volcanic system. Bull. Volcanol., 52: 355–374.

Symonds, R.B., Reed, M.H. and Rose, W.I., 1992. Origin, speciation and fluxes of trace-element gases at Augustine Volcano, Alaska: Insight into magma degassing and fumarolic processes. Geochim. Cosmochim. Acta, 56: 633–657.

Symonds, R.B., Rose, W.I., Bluth, G.J.S. and Gerlach, T.M., 1994. Volcanic-gas studies: methods, results and applications. Rev. Mineral., 26: 30: 1–66.

Thomas, E., Varekamp, J.C. and Buseck, P.R., 1982. Zinc enrichment in the phreatic ashes of Mount St. Helens, April 1980. J. Volcanol. Geotherm. Res., 12: 339–350.

Toutain, J.P., Bauborn, J.C., Le Bronec, J., Allard, P., Briole, P., Marty, B., Miele, G., Tadesco, D. and Luongo, G., 1992. Continuous monitoring of distal gas emanations at Vulcano, southern Italy. Bull. Volcanol., 54: 147–155.

Varekamp, J.C., Thomas, E., Germani, M. and Buseck, P.R., 1986. Particle geochemistry of volcanic plumes of Etna and Mount St. Helens. J. Geophys. Res., 91: 12,233–12,248.

Viglino, J.A., Harmon, R.S., Borthwick, J., Nchring, N.L., Motyka, R.J., White, L.D. and Johnston, D.A., 1985. Stable isotope evidence for a magmatic component in fumarole condensates from Augustine Volcano, Cook Inlet, Alaska. USA. Chem. Geol., 49: 141–157.

Yoder Jr., H.S. and Tilley, C.E., 1962. Origin of basalt magmas: an experimental study of natural and synthetic rock systems. J. Petrol., 3: 342–532.